ChemComm

Check for updates

Lead-free perovskites for solar cell applications: recent progress, ongoing challenges, and strategic approaches

Imtiaz Ahmed, [ID] [a] Kamal Prakash[a] and Shaikh M. Mobin [ID] *[abc]

The growing perovskite solar cells (PSC) have reached a power conversion efficiency of up to 25% within a decade and demonstrated the potential to replace traditional silicon-based solar cells. However, a major issue with perovskite solar cells regarding their practical application and commercialization is their lead-based toxicity, which has harmful effects on human health and ecological systems. Thus, lead-free perovskite solar cells have emerged as one of the most promising prospects in perovskite solar cell technology due to their non-toxic nature, optimal stability, and durability. Since their discovery, lead-free perovskite solar cells have achieved a maximum power conversion efficiency of ∼15% and still require further development. In this feature article, we review the recent developments in the field of lead-free perovskite solar cells. We emphasize the advantages and limitations of Pb-free perovskites and the current state of lead-free perovskite solar cells. Furthermore, we discuss the impact of cation and anion sites on the stability and efficiency of lead-free PSCs and provide an update on the progress of lead-free perovskites for photovoltaic applications. Designing environmentally friendly lead-free perovskite devices is an imperative goal, though it comes with significant challenges. This article provides a brief analysis of the challenges and strategies required to improve the stability and efficiency of lead-free perovskites. Finally, we summarize the review to offer a better understanding of lead-free PSCs and outline the direction for further exploration.

[a] Department of Chemistry, Indian Institute of Technology Indore, Simrol Khandwa Road, 433552, India. E-mail: xray@iiti.ac.in
[b] Center for Advanced Electronics (CAE), Indian Institute of Technology Indore, Simrol Khandwa Road, 433552, India
[c] Center for Electric Vehicle and Intelligent Transport System (CEVITS), Indian Institute of Technology Indore, Khandwa Road, Simrol, Indore 453552, India

Imtiaz Ahmed

Dr. Imtiaz Ahmed received his MSc and PhD degrees in Chemistry from the Central University of Punjab in 2018 and 2023, respectively. He served as a Postdoctoral Research Scientist at Mahidol University in Thailand and is currently a Postdoctoral Research Associate in the Department of Chemistry at the Indian Institute of Technology Indore (IITI). His research focuses on energy conversion, particularly water electrolysis (OER, CER and HER), supercapacitors, heterogeneous catalysis, and photocatalysis. He is a recipient of the Council of Scientific & Industrial Research Junior Research Fellowship Award (2018), Senior Research Fellowship Award (2021) and Postdoctoral Research Associate (2024).

Kamal Prakash

Dr. Kamal Prakash received his PhD degree in Chemistry from the Indian Institute of Technology (IIT) Roorkee, India in May 2018. Following his PhD, he worked as a Postdoctoral Fellow at the University of Houston, Texas, USA (2018–2019) and Indian Institute of Technology Ropar (2021–2022). He currently works as an NPDF fellow at IIT Indore since 2022. His current research interests focus on the design and synthesis of novel covalent organic frameworks (COFs) and their material applications.

1. Introduction

Solar energy has emerged as a powerful method of energy production that harnesses sunlight. It is expected to become a major energy source for future generations due to its unlimited and eco-friendly nature.[1] Solar power will also serve as an effective sustainable energy source to reduce dependence on traditional energy sources and help combat global warming and climate change.[2] In this regard, solar cells have been developed to convert solar energy into electric energy *via* photovoltaic (PVs) technology.[3] Solar cells possess energy bandgaps ranging from 1.1 to 1.7 eV, which is close to the ideal bandgap of 1.5 eV required for optimal solar energy conversion. Several types of solar cells have been developed for photovoltaics (PVs), including inorganic solar cells such as silicon (Si), copper indium gallium selenide (CIGS), and gallium arsenide (GaAs), as well as organic solar cells like dye-sensitized solar cells (DSSCs) and organic polymer solar cells (OPVs).[4–7] Crystalline silicon solar cells have demonstrated a power conversion efficiency of up to 26% and have gained wide recognition as the optimal solar cells in photovoltaics due to their superior electronic, optical, and thermal properties, as well as their high stability in various environmental conditions.[8] Organic solar cells are also appealing due to their low-cost production and feasible synthesis.[9] In recent years, perovskite solar cells (PSCs) have emerged as one of the most promising energy technologies, as they exhibit higher energy efficiency than other types of solar cells and offer cost-effective production with fewer and less expensive processing steps.[10] Lead-free perovskites have recently received sustained attention for applications in single-crystal X-ray detectors,[11–13] photodetection,[14,15] water detection,[16] scintillators,[17,18] and potential use in solar cells,[19–21] wireless light communication, and X-ray imaging,[22] due to their nontoxicity, low-cost, as well as excellent stability and optoelectronic properties.

Perovskite materials can be represent by the chemical formula ABX$_3$, similar to mineral perovskite calcium titanium oxide (CaTiO$_3$), where 'A' and 'B' are two positively charged cations with different sizes, while X represents the anion, mostly oxide, connected to both cations. Generally, perovskite materials have a cubic structure, in which B represents an atom surrounded by an anion octahedron in a 6-fold coordination, while A represents an atom with a 12-fold cuboctahedral coordination. Other forms of perovskite also exist with different arrangements of A and B atoms such as A1$_{x-1}$A2$_x$ and/or B1$_{y-1}$B2$_y$ configuration, in which the A and B sites change their oxidation states and coordinate with an anion (X), deviating from the ideal configuration.[23] In a perovskite-based materials, alkali metals such as Cs$^+$, Rb$^+$, and K$^+$ and divalent metal ions such as Pb^{2+}, Sn^{2+}, and Ge^{2+} are well-known as A and B cations having large size differences, while I, Br, or Cl are used as the X anion.[24] Many organic cations such as methylammonium (CH$_3$NH$_3^+$) and formamidinium (NH$_2$CHNH$_2^+$) can also be utilized for the formation of perovskites. By varying the atoms//molecules in the structure of perovskites, their properties such as superconductivity, magnetism, spin-dependent transport (spintronics), and catalytic properties can be modulated for different applications. Thus, perovskites have attracted significant attention from the scientific community for material applications.[23]

Perovskite-based solar cells exhibit high efficiency and show promise as alternative solar cells that are low-cost, lightweight, and flexible. The crystalline layers of mixed organo-metal trihalide perovskites are capable of photo-absorption in the near IR and UV-visible regions with high molar extinction coefficients and longer exciton lifetimes, resulting in improved efficiency. In 2009, Miyaska and group employed CH$_3$NH$_3$PbI$_3$ (MAPbI$_3$) and CH$_3$NH$_3$PbBr$_3$ (MAPbBr$_3$) as photosensitizers in dye-sensitized solar cells, achieving a PCE of 3.8% and 3.1%, respectively.[25] Subsequently, a lead-halide perovskite layer was coated on a TiO$_2$ film, achieving a PCE of 9.7% under 1.5 AM sunlight illumination.[26] Since then, the PCE of PSCs has increased exponentially from 3.8% to 22% within a decade, competing with the traditional Si-, CdTe-, and GaAs-based solar cells.[21] Lead halide perovskite solar cells have demonstrated a high PCE of over 25%, similar to silicon-based solar cells.[27–29] The electronic properties and photophysical of PSCs significantly depend on the crystal growth and morphology of perovskite structures. The high efficiencies of PSCs are attributed to the impressive optoelectrical properties of semiconducting organic–inorganic perovskite materials such as high optical absorption, tunable bandgap, effective photogenerated electron–hole pairs, and efficient charge transportation. Recently, perovskite/perovskite tandem solar cells and perovskite–silicon tandem solar cells achieved a PCE of 29.1% and 33.9%, respectively, surpassing silicon-based solar cells.[30,31] Additionally, PSCs can be prepared *via* low-temperature solution-based processes that are low-cost and less energy-intensive, providing the advantage of cost-effectiveness and making them significantly cheaper than traditional silicon-based solar cells. Further, PSCs can be easily fabricated or deposited *via* solution processing methods, which are favorable in large-scale manufacturing, practical application, and subsequent commercialization.[32]

Prof. Shaikh Mobin obtained his Bachelor's and Master's from Wilson College, University of Mumbai with a Major in Chemistry and PhD from Mumbai University in Chemistry. In 2012, he joined IIT Indore and is now working as a Professor in the Department of Chemistry. He has developed his multi-disciplinary research group working in a wide area of research including solid-state structural transformation, design and synthesis of new classes of MOFs and their applications in energy storage, conversion and biomedical devices, exploring metal nano-oxide materials for energy storage, conversion, optical and electro-chemical sensing, metal nano-oxide materials derived by employing metal complexes/MOFs as single-source molecular precursors as catalysts in organic transformations and developing greener c-dots for bioimaging and biomarkers. Moreover, his research group designs and synthesizes small molecules as cellular organelle targets and for docking.

Shaikh M. Mobin

However, although perovskite-based solar cells have achieved unprecedented PCEs, many concerns hinder their large-scale applications. The major concerns regarding perovskite solar cells are their long-term stability and the toxicity of lead. Also, PSCs are susceptible to environmental conditions and have a short lifetime span. Thus, different strategies have been employed to extend the stability of PVSCs for longer periods with high efficiency.[33] Modulating the components of perovskite solar cells such as mixed cation systems and surface passivation through two-dimensional (2D) perovskite integration have been introduced, which have significantly enhanced the stability and lifetimes of perovskite solar cells.[34,35] However, the presence of lead in the perovskite structure also needs to be addressed. Pb in perovskite tends to degrade and convert into a toxic product that can cause health and environmental issues.[36] Thus, lead-based PSCs are not commercially viable, motivating researchers to explore lead-free perovskites. Various metals or cations have been identified to replace Pb in perovskite solar cells based on their size, electronic configuration, and stability without compromising their impressive efficiency. These metals or cations must possess similar optoelectronic properties to perovskite solar cells such as optimal bandgap, high optical molar coefficients, longer exciton lifetimes, charge mobility, and long-term stability. Several transition metals, or lanthanides, alkaline earth metals, and p-block elements have shown the ability to substitute lead in perovskite materials.[37] Some of the examples are Sn^{2+}, Ge^{2+}, Be^{2+}, Sr^{2+}, Ba^{2+}, Ga^{2+}, In^{2+}, Bi^{3+}, Sb^{2+} Eu^{2+}, Tm^{2+}, and Yb^{2+}.[38,39] Especially, Sn/Ge-based halides, Bi/Sb-based halides and some double perovskites, some with perovskite-like structures, have shown immense potential to develop lead-free PSCs.[40]

There has been significant advancement towards lead-free perovskites, but different challenges in realizing efficient and stable PSCs are still unresolved for their real-life application. Thus, our review mainly focuses on the recent progress and advancement in the field of lead-free PSCs. Firstly, we present the requirements of lead-free perovskite solar cells and highlight the advantages and limitations of Pb alternatives in PSCs, together with synthesis of lead-free perovskites solar cells and their essential optical characteristics. Then, the impact of different cation and anion sites on Pb-free perovskite materials for application in solar cells will be discussed. The development of Sn, Ge, Bi, Sb, and double perovskites for lead-free solar cells in recent times is comprehensively described. Finally, we describe tandem solar cells and the overall challenges regarding lead-free PSCs together with a summary and brief future perspective on developing highly efficient and environmentally friendly PSCs.

2. Advantages and limitations of Pb-free perovskites for solar cells

Lead-based perovskites, although highly efficient in converting sunlight into electricity, pose significant toxicity risks, particularly if devices degrade or are disposed of improperly. Lead contamination can harm ecosystems and accumulate in living organisms, raising environmental and regulatory concerns for the widespread, large-scale deployment of this technology.[41] This has led to the emergence of alternative lead-free perovskite materials that possess low toxicity with favorable optoelectronic properties. In the search for Pb-free alternatives, materials with strong optical absorption, narrow bandgap, high charge transportation, low exciton binding energy, and robust stability are required. This can allow Pb-free materials to serve as effective absorbers in solar cells without significantly sacrificing their performance, positioning them as preferable, sustainable options for future applications. Fortunately, many low-toxicity materials with perovskite or perovskite-like structures exhibit potential for solar cell applications. Several lead-free alternatives, such as tin (Sn)-based perovskites, other structures incorporating elements such as bismuth (Bi), germanium (Ge), and antimony (Sb), defect-structured perovskites, and double perovskites, offer beneficial characteristics for photovoltaic performance and represent potential substitutes for lead in PSCs.[35,37] Sn-based perovskites exhibit high charge mobilities and longer lifetimes, resulting in a high solar to power conversion.[42] These materials can have immense potential to develop highly efficient PSCs, as seen in lead-based cells, with a much lower toxicity profile.

Researchers are keen to develop eco-friendly perovskite solar cells that can meet industry standards for efficiency in a safer way. However, although lead-free options such as Sn-based perovskites, Bi-based compounds, and Sb-based halides are less toxic than lead, they each require unique environmental consideration.[43] Tin is leading the way as one of the most commonly explored substitutes for lead-free perovskites. Sn-based perovskite structures are very similar to Pb-based perovskites and exhibit similar optoelectronic properties.[44] However, the photo efficiency of Sn-based perovskite cells are relatively lower than that of Pb-based solar cells. One major issue with Sn perovskite solar cells is that Sn(II) is readily transformed into Sn(IV) via oxidation in the presence of oxygen and moisture, which reduces its stability and performance. Ge-based perovskite materials can also serve as Pb-free alternatives due to their optimal bandgaps for solar applications.[45] However, germanium halide-based perovskites have been less investigated because Ge is a rare metal and very expensive, making it less suitable for a low-cost economy. Bismuth and antimony are also considered safer than lead, and their perovskite materials also demonstrate good stability for photovoltaic application in atmosphere conditions.[45] However, bismuth and antimony-based perovskites exhibit a low power conversion efficiency due to their bandgap defects, insufficient charge transportation and high charge recombination rate. Additionally, the mining and refining processes for bismuth and antimony result in the release of harmful byproducts, presenting a severe concern for the ecosystem if not properly controlled. This significantly hampers their scalability and cost-effectiveness for wider applications. Another type of Pb-free perovskite family is double perovskites or ordered perovskites having a combination of monovalent and trivalent cations rather than divalent cations. Double perovskites possess a three-dimensional structure

similar to ABX_3 perovskites and show impressive optoelectronic properties and charge carriers with longer lifetimes.[46] Moreover, many lead-free double perovskites based on cesium–silver–bismuth halides have been investigated due to their stability and relatively low toxicity.[47] The key problem associated with double perovskites is their large and indirect band gap, leading to high energy loss and detrimental for solar energy harvesting. Thus, double perovskites are less efficient compared to lead-based perovskites, which may result in larger panel areas needed for equivalent power, potentially increasing the resource use and environmental footprint over time. Overall, although lead-free perovskites offer an environmentally safer profile, their stability, efficiency, and sustainable production processes need to be improved for large-scale applications. Research into encapsulation methods, material recycling, and scalable production practices will be key to minimizing the environmental impact of these promising lead-free alternatives.[48,49] Finally, the move toward lead-free perovskites aligns with global goals for sustainable energy solutions, as well as regulatory trends that may eventually limit the use of hazardous materials in consumer products. Thus, lead-free options show noteworthy promise for the future of green energy technology. Fig. 1 presents a schematic illustration of Pb replacement and potential of lead-free perovskites.

3. Present status of lead-free PSCs

Lead-free perovskites have shown significant promise; however, their performance still lags behind their lead-based counterparts. This is primarily attributed to their susceptibility to oxidation, the formation of high-density defects, and rapid crystallization dynamics. These factors collectively contribute to their suboptimal photovoltaic performance, both in terms of efficiency and long-term stability. Thus, to address these challenges, extensive efforts have been undertaken, including advancements in solution processing techniques, compositional engineering strategies (such as tuning crystal dimensionality), and innovative device engineering approaches.[50,51]

Bivalent Sn is a promising candidate for replacing Pb for lead-free perovskites given that both are from the same group and possess similar electron configurations. In 2012, Chen *et al.* first developed lead-free- PSCs using $CsSnI_3$ perovskite. $CsSnI_3$ perovskite served as a direct semiconductor for Schottky solar cells with a bandgap of 1.3 eV and a PCE of nearly 1%.[52] Later, in 2014, Noel and team demonstrated a lead-free, $CH_3NH_3SnI_3$ perovskite solar cell with a PCE efficiency of 6% and high J_{sc} of 22.7 mA cm^{-2}.[53] This was a significant achievement in terms of PSC efficiency and led to the rapid development of Sn-halide perovskite solar cells, achieving the highest efficiency of 15% within a few years. However, the conversion of Sn^{2+} to Sn^{4+} *via* oxidation in Sn-halide perovskites reduces their efficiency and stability. Thus, formamidinium tin iodide ($FASnI_3$) perovskites have been widely explored considering their ability to prevent Sn oxidation and obtain a lower hole density compared to other perovskites. In recent times, highly efficient Sn-based PSCs were prepared *via* composite formation, use of additives, or surface engineering to hamper the conversion of Sn^{2+} to Sn^{4+} and enhance the charge carrier mobility, leading to PSCs with superior performances and stability. The oxidation of Sn^{2+} to Sn^{4+} is one of the major challenges limiting the stability and performance of tin-based perovskite solar cells. This is due to their increased defect density, reduced charge carrier lifetime, and accelerated material degradation. Thus, various strategies are discussed in this work to mitigate
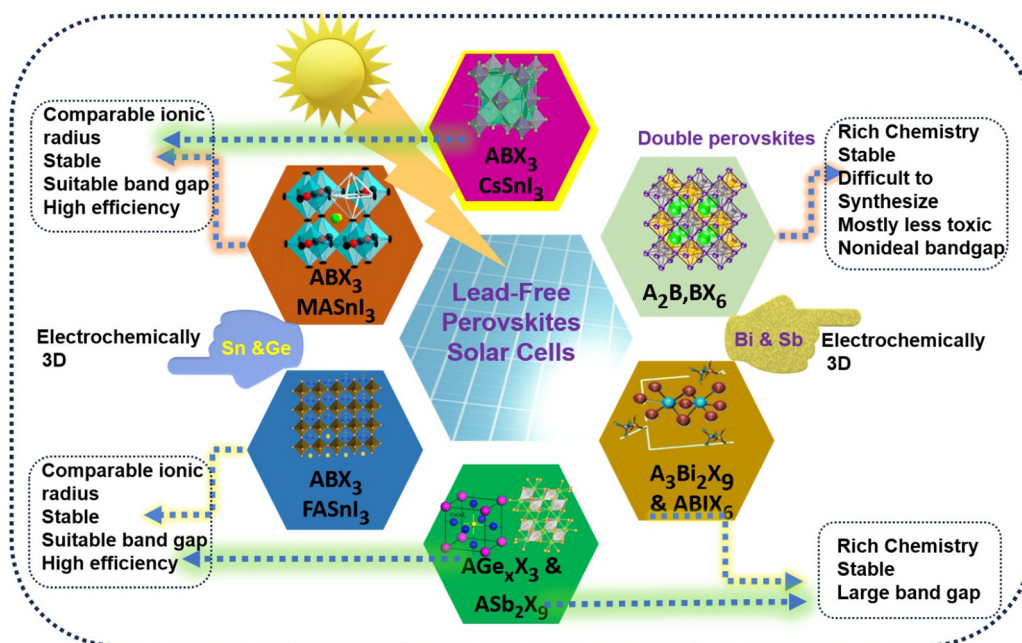

Fig. 1 Schematic of the replacement of Pb and the potential of lead-free perovskites.

these challenges. P. Wang *et al.* fabricated SnF_2 on a methyl-ammonium tin iodide ($MASnI_3$) film through insertion reactions/ ion exchange, achieving a PCE of 7.78%.[54] The large amount of SnF_2 improved the crystallinity of $MASnI_3$ and suppressed the detrimental oxidation, which allowed it to achieve a PCE of 7.78%. Further, W. Zhang *et al.* utilized dimethyl ketoxime (C_3H_7NO, DMKO) as a multifunctional additive in $CsSnI_{3-x}Br_x$ based organic-free and Pb-free based PSCs and obtained an enhanced PCE of over 11.2%.[55] The introduction of the 2D phase can enhance the crystalline 3D growth to form a unique 2D/3D microstructure to reduce the defect density and enhance the device performance. Z. Kang and coworkers remarkably enhanced the PCE of a 2D–3D tin-based perovskite heterostructure to 12.45% by simply introducing low-dimensional phases.[56] In another interesting work, the introduction of a 2D phase $FASnI_3$ structure led to an enhancement in the PCE from 9.38% to 14.81%.[57] However, although tin-based PSCs have been extensively studied, their efficiency and stability are still not comparable to that of Pb-based PSCs, and thus more efforts are required to enhance their performance. Considering elements in the same group, germanium (Ge^{2+}) can also be promising as a divalent lead alternative. Krishnamoorthy *et al.* first synthesized germanium iodide perovskite solar cells using spiro-OMeTAD and TiO_2 as the electron- and hole-selective layers, respectively.[58] Different cations of Cs, MA, and FA were employed for the synthesis of Ge-based perovskites and investigated for their potential for photovoltaic applications. In their study, $CsGeI_3$ and $MAGeI_3$ displayed PCE values of 0.11% and 0.2% for solar cells with J_{sc} values of 5.7 and 4 mA cm^{-2}, respectively. It was proven that the bandgap of $CsGeX_3$ (X = I, Br, Cl) decreases with the size of the halide-ions and only the $CsGeI_3$ perovskite has an optimal bandgap suitable for photovoltaic devices.[59] Ge-based PSCs are even more susceptible to oxidation than Sn-based devices due to the high stability of the Ge^{4+} ion *via* the inert pair effect. This leads to the poor efficiency of Ge perovskites and minimizes their application as single metallic PSCs. Thus resolve this, mixed Ge/Sn-based perovskites have been developed. The amalgamation of Ge and Sn for the fabrication of perovskite solar cells represents a new approach for boosting their stability and efficiency. In 2019, the $CsSnGeI_3$ perovskite was formed by alloying Ge(ii) in the $CsSnI_3$ perovskite composition, which showed high chemical and thermal stability and delivered a PCE of up to 7.11%.[59] Recently, ozone-exposed PEDOT:PSS was applied in a Sn–Ge mixed perovskite, improving its PCE from 6.8% to 8.1%.[60] The exposure of PEDOT:PSS to ozone optimized the band energy levels and enhanced the hole mobility, subsequently improving the PSC performance. Moreover, the PCE of Ge-based solar cells can be significantly improved by the selection of appropriate cation, mixed perovskite, and surface engineering. However, the commercialization of Ge-based perovskite solar cells is not economical considering the high cost of Ge.

Similar to Pb and Ge, Bi(iii) and Sb(iii) have also been considered possible substitutes for lead-free perovskites. As elements in group 15, Bi and Sb possess an electronic configuration similar to Pb(ii) and show high stability and non-toxic nature under atmosphere conditions.[61] In 2015, Park *et al.* initially reported $Cs_3Bi_2I_9$ PSCs with a PCE of over 1%.[62] Later in 2016, solution-processed $AgBi_2I_7$ thin films were developed by spin-coating silver, which formed pinhole-free surface morphologies and possessed a narrow band gap of 1.87 eV. The $AgBi_2I_7$-based devices produced a PCE of 1.22% with outstanding stability over 10 days under atmosphere conditions.[63] Subsequently, various compositions of silver bismuth iodide (AgBiI) were prepared using different ratios of AgI/BiI_3 and investigated for solar cells, albeit the highest efficiency of 2.31% was obtained.[64] The low efficiency of Bi-based perovskites can be rationalized in terms of their large bandgap and low-dimensional structures such as 0D and 2D. Thus, to counter the dimensionality issue, three-dimensional $AgBi_2I_7$ was formed, which showed a more suitable band gap of 1.83 eV for photovoltaics compared to the 0D $Cs_3Bi_2I_9$ (2.16) and 2D $Rb_3Bi_2I_9$ (2.10) structures.[65] Durrant and coworkers synthesized $(CH_3NH_3)_3Bi_2I_9$ films with excellent optoelectronic properties and produced a hysteresis-free, PCE of 3.17% with good reproducibility.[66] Additionally, a strategic improvement in PCE was achieved by tuning the optoelectronic properties of $Ag_aBi_bI_{a+3b}$ *via* limited anionic sulfide substitution.[67] The effect of the sulfide anion on these compositions was seen by the adjustment in valence band edge by 0.1–0.3 eV, and subsequently the corresponding PCE. Thus, a record PCE value of $5.44 \pm 0.07\%$ for Bi-based perovskites was achieved under 1 sun irradiation with a J_{sc} value of 14.6 mAcm^{-2} and excellent stability under ambient conditions for over a month. This indicated that optimizing the composition of Bi-based PSCs substantially improved their performance. Compared to other metals, Sb is a naturally occurring metal and cheaper, which is capable of achieving cost-effective PSCs by replacing Pb. Hence, many Sb-based perovskites have been investigated as capable candidates for solar cells.[68] In 2015, Mitzi *et al.* pioneered antimony-based lead-free PSCs by developing a 2D layered perovskite derivative, $Cs_3Sb_2I_9$.[69] It exhibited a direct bandgap of 2.05 eV and similar photo-absorption as $CH_3NH_3PbI_3$, making it very promising for optoelectronics applications. T. Kirchartz *et al.* prepared the $(CH_3NH_3)_3Sb_2I_9$ perovskite material and utilized it as an absorbing layer in a heterojunction solar cell, achieving a PCE of 0.5% with low photocurrent densities.[70] Further, Bhoopathi *et al.* and S. Chatterji lowered the optical band gap of $(CH_3NH_3)_3Sb_2I_9$ perovskite solar cells and improved the PCE significantly.[71,72] In another work, our group fabricated a smooth layer of $(NH_4)_3Sb_2I_9$ perovskite material in a PCS device, achieving a PCE of 0.42% with a V_{oc} of 945 mV.[72] In a recent study, theoretical calculations of the PCE of Sb-based PSCs were performed, which suggested that stable and highly efficient Sb-based PSCs may achieve a PCE of 23.10% by optimizing their perovskite layer thickness, doping concentration or density defect, *etc*.[73] However, to replace Pb in PSCs, more work is required to make Bi and Sb compatible.

Further, double perovskites have emerged as a fascinating and alternative approach in the field of lead-free PSCs.[74] In lead-free double perovskites, two Pb^{2+} positions are replaced with two different cations with +1 and +3 valency and form an $A_2B^{1+}B^{3+}X_6$ structure. Many double perovskites with the $A_2B^{1+}B^{3+}X_6$ structure have been developed with Cs, Cu, and MA at the A position, Ag^+, In^+, Na^+, and K^+ at B^+, Bi^{3+}, Sb^{3+}, and
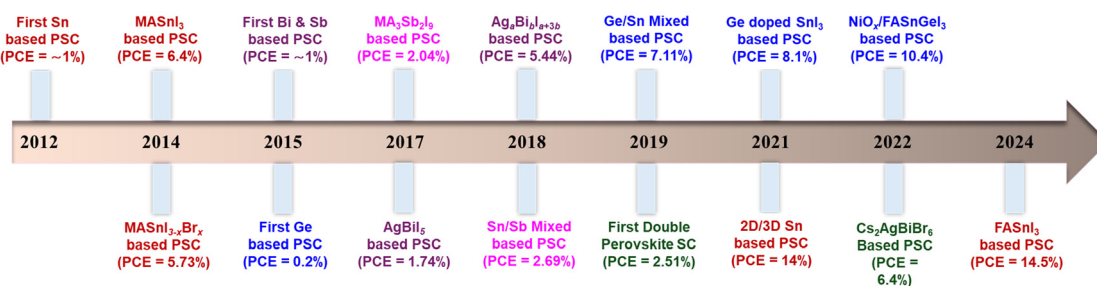
Fig. 2 Representative examples of lead-free perovskites and their PCE values over the years.

In^{3+} at the B^{3+} position and X as halide ions.[75] Double perovskites possess unique properties such as optimal bandgap, high thermal stability, increased charge mobility, and low exciton binding energy, making them favorable for photo applications. Fig. 2 presents the development of lead-free perovskites and their PCE values over the years.

4. Synthesis of lead-free perovskites for solar cells

Several methods are available to develop lead-free perovskite materials; the most popular are solution processing, vapor phase deposition, solid-state synthesis, and hydrothermal/solvothermal synthesis. The choice of a particular method depends on which form of perovskite material needs to be synthesized, such as nanocrystal, colloidal, or thin films. Generally, single-crystal perovskites are developed *via* the temperature-lowering method, traditional solvothermal method, and antisolvent crystallization. In the temperature-lowering method, single crystals of perovskite are formed at a temperature lower than typically preferred. Mitzi *et al.* first reported the synthesis of tin-based single crystals $(C_4H_9NH_3)_2(CH_3NH_3)_{n-1}Sn_nI_{3n+1}$ (n = 1–5) using the temperature-lowering crystallization method, keeping the temperature rate between 2 °C to 5 °C per hour.[76] The double perovskite Cs_2Ag^I-$Bi^{III}Br_6$ was prepared by heating the solution at 110 °C for 2 h and cooling it to room temperature. It exhibited similar photovoltaic properties to $(MA)PbI_3$ and $(MA)PbBr_3$, suggesting its photo-based applications without having a toxic element. Compared to the temperature-lowering method, anti-solvent crystallization can be performed under ambient conditions, which involves the addition of a second solvent to reduce the solubility of the solution and form single crystal perovskites. This method is also called precipitation, desolvation, or solvent displacement. Chen *et al.* utilized acetic acid (HAc) as an anti-solvent to synthesize tin-based perovskites, which increased the nucleation growth of the precursors *via* salting-out crystallization. Antisolvent and primary solvent DMSO form hydrogen bonds to lessen the solvation of the precursor and enhance the effective concentration to give a crystallized form from the solution.[77] Chu and coworkers applied chlorobenzene, isopropyl alcohol, and anisole as antisolvents to prepare $Cs_3Sb_2Cl_xI_{9-x}$ perovskite films. Among them, anisole as a green antisolvent achieved a dense surface morphology for

perovskite single crystals with high crystallinity and photo-absorption ability. Thus, the Sb-perovskite with anisole showed a superior photovoltaic performance with a PCE of 2.07%.

Further, lead-free perovskite nanocrystals can be formed *via* either the hot injection method or recrystallization technique. Between them, the hot injection method is preferred because the size and morphology of perovskite colloids can be modulated by varying the reaction conditions such as precursor concentration, temperature, and time. The formation of $CsSnX_3$ (X = Cl, $Cl_{0.5}Br_{0.5}$, Br, $Br_{0.5}I_{0.5}$, I) perovskite nanocrystals was attempted from Cs_2CO_3 and SnX_2 unsuccessfully due to the formation of CsX precipitation. For the synthesis of $CsSnX_3$ perovskite nanocrystals, SnX_2 was dissolved in reducing tri-n-octylphosphine solvent and injected into a Cs_2CO_3 solution containing oleic acid and oleylamine at 170 °C, which resulted in the formation of highly stable $CsSnX_3$ colloidal nanocrystals, as confirmed by powder X-ray diffraction (PXRD).[78] Moreover, Cs_2SnI_6 NCs were developed *via* the hot injection method and could be transformed into different structural shapes, such as spherical quantum dots, nanorods, and nanowires, by changing reaction time and ligands. Oleic acid and oleylamine helped form high-quality perovskite nanocrystals.[79] Likewise, colloidal $Cs_3Sb_2I_9$ nanocrystals were also prepared *via* the hot injection method. In this context, Bi-based double perovskite nanocrystals, $Cs_2AgIn_{0.9}$-$Bi_{0.1}Cl_6$, were obtained using CsCl, AgCl, $InCl_3$, and $BiCl_3$ solution in DMSO.[80] This solution was further injected into isopropanol antisolvent, and the NCs were obtained by centrifugation. However, these two methods are the only methods available to synthesize lead-free halide perovskite colloids, and thus other techniques need to be developed.

Therefore, lead-free perovskites, particularly Sn-based perovskite thin films for PSC application, are synthesized through solution processing methods such as one- or two-step deposition and vapour deposition methods.[81–83] Compared to lead-based perovskites, lead-free perovskites are mostly synthesized using organic cations such as MA and FA, inorganic cations such as Cs^+, Rb^+, and other alkali cations that occupy the A-position. In this regard, the solution processing and vapour deposition methods are the most compatible with forming lead-free perovskites for perovskite solar cells. The one-step solution method is widely considered for the synthesis of tin-based perovskites. SnI_2 has low solubility in commonly used solvents such as *N*,*N*-dimethylformamide (DMF) and crystallizes faster

that its Pb-counterparts. Thus, single solvents such as DMSO were strategically explored to develop Sn-based perovskite films through a one-step spin-coating method.[84] The precursor SnI_2 formed a stable intermediate with DMSO to resist the faster crystallization process and produce a high-quality perovskite thin film. An $FA_{0.75}MA_{0.25}SnI_3$ perovskite thin film was fabricated using chlorobenzene antisolvent with a high film coverage and reduced pinhole generation, which achieved a PCE of 6.6%.[85] Further, an $FA_{0.75}MA_{0.25}SnI_3$ perovskite thin film was fabricated using various antisolvents for PSC applications. Besides the one-step solution method, the two-step solution method can also be employed to develop lead-based perovskites, but it is not suitable for Sn-based perovskites. Zhu and group first introduced a two-step process for Sn-based PSCs by using SnI_2 in trimethylaluminum (TMA) solution with a lower concentration of SnF_2. TMA forms an SnI_2-TMA complex, which delays the fast reaction of FAI and SnI_2 and enhances the perovskite crystallization by preventing SnF_2 segregation. Thus, an improved SnI_2 film with the maximum coverage was obtained, which achieved a superior efficiency of 7.09%.[86] A bismuth-based $(CH_3NH_3)_3Bi_2I_9$ (MBI) PSC was developed via a two-step sequential solution method using a rutile TiO_2 layer and electron transporting layer (ETL). The photovoltaic result exhibited a PCE of 0.14% for this PCS with excellent stability up to 67 days under ambient conditions.[87] Recently, Han and co-workers prepared Sn-based PSCs using DMSO as the solvent. The developed Sn films had a uniform morphology and showed a PCE of over 10%.[88]

Another strategy to achieve high-quality lead-free perovskite films is the vapor deposition method. There are several examples of the preparation of Sn-based films through the vapor-assisted method. It produces a uniform and smooth morphology thin-film without the use of any incompatible solvent. A lead-free $MASnI_3$ film was prepared for the first time via a low-temperature vapor-assisted solution process (LT-VASP).[89] The resulting high-quality Sn film-based PSC achieved a PCE value of 1.86%. This work suggested that the substrate temperature plays an important role in obtaining high surface coverage and excellent uniformity for thin films. Wang et al. utilized a sequential-vapor-deposition procedure to prepare double perovskite $Cs_2AgBiBr_6$ thin films for photovoltaic application.[90] The $Cs_2AgBiBr_6$ thin films exhibited large grain sizes and uniform and smooth surface properties. Consequently, the $Cs_2AgBiBr_6$ thin film-based PSC device achieved a PCE value of 1.37% with high stability. The feasibility of the vapor deposition method to fabricate high-quality thin films leads the way for the further exploration of various PSC devices based on lead-free perovskites. Finally, the main reason behind using different methods for thin-film synthesis is to optimize the quality of thin films in terms of their crystallinity, thickness, grain size, phase purity, and crystal orientation to improve the PCE of solar cells. However, the photovoltaic efficiency of lead-free perovskite solar cells is still lower compared to that of lead-based PSCs, and thus new synthetic strategies still need to be explored.

5. Essential optical characteristics of lead-free perovskite solar cells

To replace lead perovskite solar cells with lead-free halide perovskites and achieve high PCEs, certain optoelectronic properties need to be enhanced, such as the absorption coefficient, charge mobility, carrier lifetime, small exciton binding energy of photogenerated electrons, and low trap density. The optical properties of perovskites depend on the high electronic dimensionality, metal electronic configuration, and nature of their organic cations and halides. The structural dimensionality of perovskite materials has a large impact on their photovoltaic performance. In the case of Pb-based perovskites, their bandgap increases with a reduction in structure dimensionality from 3D to 0D. It has been found that 0D and 1D perovskites possess large bandgaps and localized band edges, which are not beneficial for photovoltaic application, while 2D perovskite film growth must be aligned parallel to the layers to facilitate effective charge generation and transportation. Alternatively, 3D perovskites are more promising as absorber materials for photovoltaics due to their optimal bandgap, flat band edges, high absorption coefficient and high charge mobility. This indicates that the 3D structure of lead-free halide perovskites should be highly desirable solar cell absorber materials.

Moreover, high photo absorption is very important to design efficient PSC devices. Pb-based halide perovskites display high optical absorption coefficients with a layer thickness of ≈ 500 nm, far ahead of traditional inorganic thin-film solar cell technologies.[91,92] In the case of lead-free perovskite solar cells, Sn^{2+} has the same electronic configurations and structural properties as Pb^{2+}, and thus Sn also exhibits high absorption upon solar irradiation for PSC application. $MASnI_3$ perovskite thin films displayed a direct band gap of 1.3 eV and a PL emission band at 950 nm with high absorption.[93] Replacing MA with the ratio of FA led to different emissions corresponding to their ratio in a PSC cell.[94] High charge mobility of photogenerated electron and holes is essential to obtain efficient thin-film solar cells given that it increases the carrier lifetimes and reduces their recombination rate. $MASnI_3$ and $CsSnI_3$ exhibited high electron mobilities of 2320 and 536 cm^2 V^{-1} s and produced power to a conversion efficiency of 6.63% and 3.79%, respectively.[95,96] Similarly, PSC devices with a low trap density demonstrate high efficiency due to their facile charge carrier transportation and improved stability. The $FASnI_3$ material exhibits lower charge-carrier mobility than $CsSnI_3$ and $MASnI_3$, but PSC devices based on it showed high efficiency (PCE = 12%) due to its low trap density.[97] $FASnI_3$ perovskites also show excellent thermal stability compared to others, although they have lower conductivity than $MASnI_3$. Moreover, the doping of different ions in hybrid halide perovskites has a profound impact on the absorption and band gap of perovskite solar cells. Halide hybrid perovskites $MASnI_{3-x}Br_x$ exhibited tuned optical properties as PL emission of $MASnBr_3$, $MASnI_2Br$, and $MASnIBr_2$ appeared at 577, 795, and 708 nm with modulated band gap edges, respectively.[93] This also impacted the PCE given that the $MASnIBr_2$-based device delivered the best PCE

value of 5.73% under solar illumination, while $CH_3NH_3SnI_3$ showed a PCE of 5.23%. Similar to Sn(II), Ge is also a group IVA element and a potential candidate for the fabrication of perovskite solar cells. An investigation into a series of Ge-based perovskites, $CsGeI_3$, $MAGeI_3$, and $FAGeI_3$, depicted that the structural dimensionality of $AGeI_3$ is completely different from each other due to their cation size, and they exhibit direct band gaps of 1.63, 2.0, and 2.35 eV, respectively.[58] The optical properties of $AGeI_3$ are suitable for perovskites solar cell application given that they exhibit strong absorption in the range of 400–600 nm together with sharp band edges. However, the PCE of $MAGeI_3$ and $CsGeI_3$ were found to be 0.20% and 0.11%, which is relatively lower than that of their Sn-based counterparts, and also indicated that band gap tuning by changing the cation can improve their photovoltaic performance.[58] The photovoltaic performance of tin-based PSCs is hampered by the facile oxidation of Sn(II) to Sn(IV), which degrades the absorber perovskite material significantly. In this context, a change in the dimensionality of the structure readily from 3D to 2D or mixed 2D and 3D Sn perovskites can lead to high-stability perovskites, subsequently improving the PCE.[98,99]

Besides Sn and Ge, Bi^{3+} and Sb^{3+} may be alternatives to lead-free perovskites due to their low toxicity and similar electron configuration. Generally, Bi and Sb form an $A_3B_2X_9$ perovskite structure, where the B-positions are occupied in the perovskites. $A_3B_2X_9$ perovskites mostly exhibit wider band gaps, generally larger than 1.9 eV, and large absorption coefficients in the visible region and possess excellent stability in air and moisture. $A_3B_2X_9$ perovskites such as $MA_3Bi_2I_9$, $Cs_3Bi_2I_9$, and $MA_3Bi_2I_9$, were formed *via* a solution processing method and exhibited weak absorption, high exciton binding energies, and low charge carrier mobilities. Their corresponding photovoltaic devices produced low efficiency, and the highest PCE of only 1.09% was obtained for $Cs_3Bi_2I_9$.[62] Later, ABi_3I_{10} perovskites were also developed, and their absorption and band structure were also adjusted by varying their cations (A = MA, FA, and Cs).[100] These perovskites demonstrated good stability in air and were utilized as light absorbers for solar cells devices. Among them, $CsBi_3I_{10}$ achieved the highest efficiency of 1.51% due to its maximum light absorption and narrow bandgap. The bismuth-based perovskite $Cs_3Sb_2I_9$ was explored for photovoltaic applications due to its layered structure and high electron and hole mobility. The $Cs_3Sb_2I_9$-based photovoltaic devices exhibited a PCE of less than 1%, which can be rationalized in terms of their deep level defects in a layered structure.[69] Similarly, $MA_3Sb_2I_9^-$ based thin films exhibited a PCE of 0.5% despite having a suitable band gap of 2.14 eV.[70] Sb-based perovskites have poor morphology and excessive halide ions, which disturb their crystalline growth, resulting in low performance. Thus, the optimization of the contact layers and morphology of Sb-based perovskites can lead to a high power conversion efficiency.[101]

In the case of double perovskites, the $Cs_2AgBiBr_6$ perovskite was exploited due to its good optoelectronic properties and stability under ambient conditions. The $Cs_2AgBiBr_6$ perovskite has good crystallinity, narrow band gap, longer carrier lifetime, and high charge mobility. Thus, it showed an indirect bandgap

of 1.95 eV with a photoluminescence (PL) lifetime of *ca.* 660 and high stability, which are beneficial for photovoltaic studies.[102] Bein and coworkers synthesized a high-quality $Cs_2AgBiBr_6$ thin film using a one-step method and used it as an absorber material in PSC devices, obtaining a PCE of 2.5%.[103] Shao *et al.* also developed a crystalline $Cs_2AgBiBr_6$ film with a smooth morphology and large grain structure *via* an antisolvent crystallization and annealing method, which showed an efficiency of 2.23%.[104] In another work, the optical properties of the Cs_2Ag-$BiBr_6$ perovskite were enhanced by introducing an N719 dye interlayer. The incorporation of the dye increased the photo absorption, constructed a suitable band structure, and reduced the charge recombination rate, consequently improving its PCE up to 2.84%, which is higher than that of previously reported $Cs_2AgBiBr_6$-based PSCs.[104] Thus, to achieve high efficiency for double perovskites, it is necessary to apply doping or alloying techniques effectively to improve their optoelectronic properties.

6. Importance of compositional engineering of perovskites in terms of cation and anion sites

Perovskite materials with different crystal structures are known to be fascinating materials due to their unique properties and versatile applications in various fields such as solar cells, sensing, catalysis, fuel cells, and energy storage. Generally, perovskite structures are comprised of two cation sites, A and B, while one anion site X, allowing the development of a library of perovskite materials with different compositions and tuning of their electronic and optical properties. Compositional engineering of perovskites using different types of cations and anions plays an important role in optimizing their performance, stability, and functionality for a particular application. The efficiency of perovskite solar cells can also be affected by the compositional engineering of perovskites. Herein, we delve into the importance of compositional engineering, providing examples and applications to underscore its transformative role in solar cells.

6.1. Impact of the cation (A site) in Pb-free perovskites

Lead-free perovskites can assume various geometries depending on their synthesis methods and compositional variations. In terms of high carrier mobility, optimum direct bandgap, and tolerance to defects due to its higher dielectric constant, theoretical studies reveal that the corner-sharing 2D-structure of octahedron layers is more favorable compared to the face-sharing 0D-structure of octahedron dimers.[69] Considering antimony (Sb) as an example, the layered phase of $A_3Sb_2X_9$ is challenging to achieve through conventional solution processing. Therefore, innovative solution-processable approaches must be explored and developed to synthesize layered perovskites. The properties of lead-free based perovskites can be finely tuned by varying the concentrations of their cations. Notably, the structure of perovskites is significantly influenced by the effective ionic radius of their cation, underscoring its critical role in determining the crystallographic arrangement of these material.[105] In the case of

inorganic cations, density functional theory calculations revealed that the formation energies of the two structural forms of Sb-based perovskites differ by only 0.1 eV. Consequently, the specific synthesis conditions play a decisive role in determining which structural form is obtained.[106] Inorganic perovskites are an emerging class of halide perovskites with enhanced stability against oxygen, moisture, and elevated temperatures. In the case of organic cations, methylammonium is a bulky group in hybrid inorganic–organic Sb perovskites ($MA_3Sb_2X_9$). To get a layered structure, the stoichiometries of the halides in mixed perovskites must be varied. To adopt a well-stabilized structure in a perovskite crystal, it must possess an optimal tolerance factor.[107] Accordingly, incorporating smaller cations in the structure has been shown to be an effective strategy for attaining the optimal tolerance factor.[108] When comparing organic and inorganic cations, organic cations, despite being bulkier (*e.g.*, methylammonium, formamidinium, ethylammonium, and guanidinium), demonstrate superior stability and performances compared to other monovalent inorganic cations such as Cs, Rb, K, Na.[22,69,109,110] Cs as an inorganic cation provides more thermal and chemical stability to perovskite materials. Thus, Cs-based perovskite structures have been widely explored. The incorporation of the rubidium cation is beneficial for the phase stability of perovskites. The Rb^+ ion effectively increases the grain boundaries of perovskite materials, which readily reduces the non-radiative recombination and enhances the charge mobility.[111] Further, organic cations such as methylammonium ($CH_3NH_3^+$) and formamidinium ($CH(NH_2)_2^+$) were mainly utilized for the formation of hybrid perovskites. MA-based perovskite materials tend to show high excellent optoelectronic properties with excellent PCE values but are often thermally unstable. Meanwhile, FA-based perovskites offer high thermal stability but are fragile to phase instability, limiting their PCE performance. However, the optimized combination of MA and FA in perovskite solar cells has been investigated to improve their performance. Thus, the variation of the A-site cation promises significant opportunities for the development of novel materials through different combinations in double and triple-cation systems. Weak hydrogen bonding interactions and cation size contribute to the structural cohesion between the inorganic framework and the A-site cation, where dipole–dipole interactions are essential in driving the structures toward their most thermodynamically stable configurations. In this context, Ozorio *et al.* described the role of the A-cations in the polymorphic stability and optoelectronic properties of lead-free $ASnI_3$ perovskites.[112]

6.2. Impact of the cation (B site) in Pb-free perovskites

In recent years, B-site doping has emerged as the most effective and extensively adopted strategy for enhancing the performance of perovskite solar cells (PSCs). This approach has been instrumental in achieving high PCEs and improved stability. By modifying the B-site composition, the optoelectronic properties and band structure of perovskite materials can be precisely tailored, enabling optimized device performances. The limited substitution of divalent cations at the B-site with either heterovalent or homovalent ions has been proven to be an effective strategy for producing high-quality perovskite materials. As described in the previous section, this approach not only reduces the reliance on toxic elements but also induces passivation effects at the grain boundaries and surfaces. It enhances the crystallinity of perovskites by increasing their grain size, thereby reducing their trap-state density and grain boundaries. These improvements contribute to lower energy losses and reduced charge recombination at the interfaces between the perovskite layer and the corresponding charge-transport layers, ultimately enhancing the device performance.[113] This strategy enables precise modulation of the bandgap energy to achieve desired values, ensuring optimal alignment with the energy levels of adjacent layers for specific applications.[114] B-site dopants, including group IIIA to VA metal ions, transition metal ions, alkaline-earth metals, and lanthanides, play a noteworthy role in enhancing the stability and photovoltaic performance of perovskite-based devices. The incorporation of these dopants offers promising opportunities to improve the material properties and device efficiencies through the B-site doping strategy.

6.3. Impact of the anion (X-site) in lead-free perovskites

To maintain charge neutrality between the anions and cations, halide ions play a crucial role, and due to their suitable effective ionic radii, they have been highly explored. The bandgap typically decreases as the electronegativity difference between the constituent cations and anions decreases.[115] The bandgap decreases linearly from Cl to Br to I, and thus halides with lower electronegativity exhibit a bandgap more suitable for absorbing a substantial portion of the solar spectrum. Research on lead-free perovskites suggests that directly substituting lead with alternative metal cations often results in a reduced device efficiency. Sn–Pb-based perovskites show great potential for achieving relatively high efficiency however, tin (Sn) still faces significant stability challenges even it may have similar properties. The anion (X-site) in lead-free perovskites significantly influences their structural, and optical electronic properties. The anion (X-site) plays a vital role in determining the physical and functional properties of lead-free perovskites, making its selection a crucial aspect in material design. The key highlights responsible for the impact of the anion on the X-site in lead-free perovskites are as follows:

(a) The nature of the anion affects the bandgap, with larger and less electronegative anions typically resulting in narrower bandgaps, enhancing light absorption in the visible spectrum. (b) Anion selection can impact the overall stability of the perovskite structure. For instance, halides such as Cl^-, Br^-, and I^- play critical roles in stabilizing the crystal lattice, but their differing ionic radii and electronegativities influence the tolerance factors and defect formation. (c) The anion determines the defect levels and density of trap states, influencing the charge carrier recombination rates and transport properties. For example, halides with lower electronegativity such as I^- are more prone to forming shallow defect levels. (d) The anion influences the phase stability of lead-free perovskites, particularly under environmental stressors such as moisture,

light, and heat. Mixed halides such as I^-/Br^- can enhance the phase stability and mitigate degradation. (e) Anions directly impact the optical absorption, emission spectra, and device efficiency. Thus, optimizing the anion composition is critical to achieving high-performance materials for photovoltaic and optoelectronic applications.

The stability and efficiency of lead-free perovskite solar cells (PSCs) are significantly influenced by the choice of cations and anions in the perovskite structure. The A-site in perovskites (ABX_3) is typically occupied by organic cations such as MA^+ (methylammonium) and FA^+ (formamidinium), or inorganic cations such as Cs^+. In lead-free PSCs, the choice of A-site cation affects their structural stability and bandgap. Inorganic cations such as Cs^+ mainly enhance the thermal stability but may increase the bandgap, reducing the light absorption, while FA^+/MA^+ help to increase the efficiency due to their better light absorption but may compromise the thermal and moisture stability. B-site cations of less toxic elements such as Sn^{2+}, Ge^{2+}, Bi^{2+}, and Sb^{2+} can be used to replace the toxic Pb^{2+}, which directly impact the electronic properties and stability. These elements may offer high efficiency, suitable bandgaps and improve the stability. Alternatively, the X-site anions are typically occupied by different halides such as I^-, Br^- and Cl^-, which affect the bandgap, charge carrier mobility, and stability. Considering I^-, it generally enables high efficiency and provides a narrow bandgap, while Br^-/Cl^- increase the band gap but improve the stability. We recognize that challenges related to stability and efficiency still persist. Thus, to address these issues, several strategies can be implemented, including cation and anion engineering, which involves tailoring the composition of the A/B-sites, as well as defect passivation and dimensional engineering, such as utilizing 2D/3D hybrid structures. These approaches aim to enhance the stability without compromising the efficiency, which are thoroughly discussed in the "Challenges and strategies" section.

7. Recent development of Pb-free perovskite materials for solar cells

To achieve the maximum solar conversion efficiency, the materials involved in constructing photovoltaics must have outstanding carrier transfer kinetics, tunable bandgap, appropriate band structure, and long length for the diffusion of carriers. Regarding the absorption of solar energy, the bandgap of photovoltaic-like materials is an important parameter. The PCE of lead-based PSCs is strongly influenced by the electronic structure of lead (Pb). Specifically, the 6p orbitals of the Pb atoms play a critical role in determining the band structure of perovskite materials. Consequently, alternative elements proposed to substitute for Pb should exhibit chemical compatibility with the perovskite structure to maintain the stability and optimal electronic properties of the material. Macdonald[116] et al. recapitulate the evolution of Sn-PSCs, including early progress to the state-of-the-art approaches benefitting the stability of devices. As is known, Pb is located in period 4, group 14 of the periodic table, and thus the most promising candidates for Pb substitution are elements from group 14, which share similar chemical properties. Additionally, elements from group15, such as bismuth (Bi) and antimony (Sb), with comparable electronic configurations and other less toxic and sustainable metals may also be considered as potential alternatives.[92] To mitigate the toxicity concerns associated with lead (Pb), it is common to partially or completely replace Pb with alternative metals in the perovskite structure.[117,118] Hence in this section, we explore the numerous alternatives to Pb perovskites for solar cell application. Among the commonly studied elements for the substitution of lead (Pb), including Sn, Ge, Sb, Bi, and Cu, tin has emerged as the most promising candidate in recent years.[53,71,119–122]

7.1. Sn-based perovskite solar cells

Sn-based perovskites have the general formula of ABX_3, where A represents organic/inorganic cations such as methylammonium (MA), formamidinium (FA), and cesium (Cs), B represents Sn, and X is a halide ion (i.e., Cl, Br, I). Sn-based PSCs mainly possess MA and FA cations in their structure to get highly efficient PSCs. Thus, the resulting crystal structures are primarily observed in either the orthorhombic $Amm2$ or cubic $Pm3m$ phase. Sn forms a traditional perovskite because the A-cations are situated at eight corners of the cubic units to occupy the cavity and metals have 6-coordinations fold with corner-sharing $[SnX_6]$ octahedra.[123] Similar to Pb, Sn perovskites display excellent optoelectronic properties compared to other perovskite-based materials. Sn-based perovskites exhibit higher charge transportation and a narrow optical band gap relative to Pb-based perovskites. According to both experimental observations and theoretical calculations, the bandgaps of Sn^{2+}-based perovskites are in the range of 0.75–1.3 eV, positioning them as promising candidates for photovoltaic applications. In addition to their suitable bandgap, Sn-based perovskites exhibit several advantageous properties, including high absorption coefficients, direct bandgaps, low exciton binding energies, and high charge carrier mobilities.[124,125] Some of the best of Sn-based perovskites are $CsSnI_3$, $MASnI_3$, and $FASnI_3$, which will be discussed next.

7.1.1. $CsSnI_3$. Pb^{2+} and Sn^{2+} have the same electronic configurations, similar coordination type, crystal structures, and comparable ionic radii, and therefore Sn seems to be an alternative to Pb, which can balance the charge and coordination number in a lead-free perovskite structure (Fig. 3a).[126] Two primary techniques have been explored for fabricating Sn-based solar cells. The first is the vacuum deposition method, which was reported by Chen et al. in 2012. A Schottky heterojunction cell was developed by fabricating a $CsSnI_3$ thin film to investigate the charge separation; however, the resulting device demonstrated a relatively low efficiency of only 0.9%. Later, in 2014, Noel et al. employed a spin-coating technique to prepare $CH_3NH_3SnI_3$ films, achieving a significantly higher efficiency of 6.4%.[52,53] $CsSnX_3$ compounds with iodide or bromide ions exhibit a lower-symmetry orthorhombic phase ($Pnma$),[78] while $CsSnCl_3$ nanocrystals acquire a cubic perovskite structure ($Pm3m$), differing from the orthorhombic phase of $CsPbX_3$.[127] However, additional research is warranted, given that some

studies suggest that $CsSnBr_3$ quantum rods may also adopt a cubic phase, which contradicts earlier observations.[128] Furthermore, substituting Sn ions for Pb in $CsPbI_3$ yields $CsSnI_3$ perovskites that exist in various polymorphic forms.[129] Ganesan *et al.* reported the synthesis of high band gap cesium-doped lead-free perovskite nanocrystals for solar cell applications. Cs_2SnX_6 represents a defect-structured perovskite possessing a cubic configuration, where half of the B sites are vacant, forming an $[SnX_6]$ isolated octahedral structure. In this structure, cesium fills the spaces between the $[SnX_6]$ octahedra in a 12-fold coordination with X atoms, as illustrated in Fig. 3b. The incorporation of mixed cations at the A position of $[(MA_{0.5}Cs_{0.5})_2SnCl_6]$ significantly enhances the stability, reducing the degradation process compared to Cs_2SnCl_6 and MA_2SnCl_6.[130] Hossain *et al.* investigated the efficiency of $CsSnI_3$ PSCs upon tuning the electron transport layer (ETL) and hole transport layer (HTL) using theoretical simulations.[131] Different combinations of HTLs were studied and the configuration of ITO-PCBM/$CsSnI_3$/CFTS/Se showed a PSCs of 24.73% with a fill factor (FF) of 83.46% and J_{sc} of 33.99 mA cm^{-2}, as shown in Fig. 3c and d.

7.1.2. MASnI$_3$. This type of Pb-free perovskite was first discovered in 1970 and reported for PSC application in 2014.[53] F. Hao first described an $MASnI_3$-based perovskite as a light absorber in photovoltaic devices. $MASnI_3$ features a band edge of 1.3 eV, which can be further manipulated by incorporating different halides (X = I or Br), and therefore a perfect contender for the fabrication of single junction SCs.[93] The $CH_3NH_3SnI_{3-x}Br_x$ PSC exhibited a PCE value of 5.73% and was termed as the first step towards low-cost, eco-friendly solar cells. Further, Nguyen *et al.* improved the performance of $FA_xMA_{1-x}SnI_3$ PSCs by varying the ratio of different organic ligands. An increase in the content of FA cation in $MASnI_3$ led to high crystallinity, a red shift in its absorption profile, and a more aligned band structure, significantly enhancing the charge carrier mobility and exciton lifetimes at the interfaces. Thus, $FA_{0.75}MA_{0.25}SnI_3$ represents the best PSC cell, giving an efficiency of 5.37%.[132] Apparently, the stability of $MASnI_3$ can be optimized by applying a DMSO-DMF solvent system. $MASn(I_{1-x}Br_x)_3$ thin films exhibited an excellent morphological structure of uniform grain sizes using a 4 : 1 (v/v) mixture of DMSO and DMF. Further, an increase in the Br content reduced the charge recombination rate and aligned the band structure for PV application. Hence, $MASn(I_{0.33}Br_{0.67})_3$ exhibited an improved PCE by up to 3.2%.[133] For the first time, Wang *et al.* reported a synthetic strategy for fabricating $MASnI_3$ perovskite films using ion exchange/insertion reactions tailored for solar cells. By effectively controlling the crystallization and nucleation processes of $MASnI_3$, they attained a highly uniform and pinhole-free perovskite structure. This advancement enabled a PCE value of 7.78%, marking the highest value for $MASnI_3$-based solar cells to date, with excellent reproducibility and stability. The *J–V* curves and histograms of PCEs for 30 devices prepared using $MASnI_3$ films are presented in Fig. 4a and b, respectively.[54]
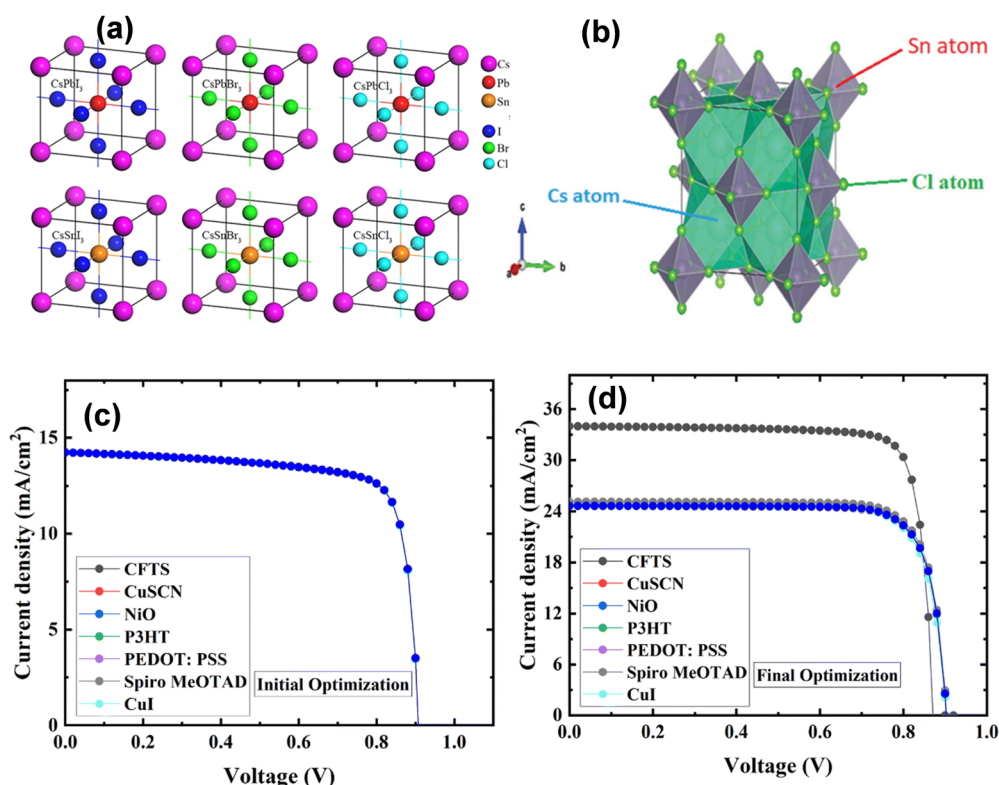

Fig. 3 Representation of unit cells of $CsBX_3$ (B = Pb and Sn) composed of different halide anions. Reproduced with permission from ref. 126, copyright 2017, Nature Scientific Reports. (b) Schematic of the crystal structure of defect perovskite Cs_2SnCl_6 (green color represents Cl atoms, while Cs atoms are positioned at the interstitial spaces). Reproduced with permission from ref. 130, copyright 2019, RSC. (c) and (d) Current density–voltage curve of the initial and final optimized structure of ITO/PCBM/$CsSnI_3$/HTL/Se, respectively. Reproduced with permission from ref. 131, copyright 2023, RSC.
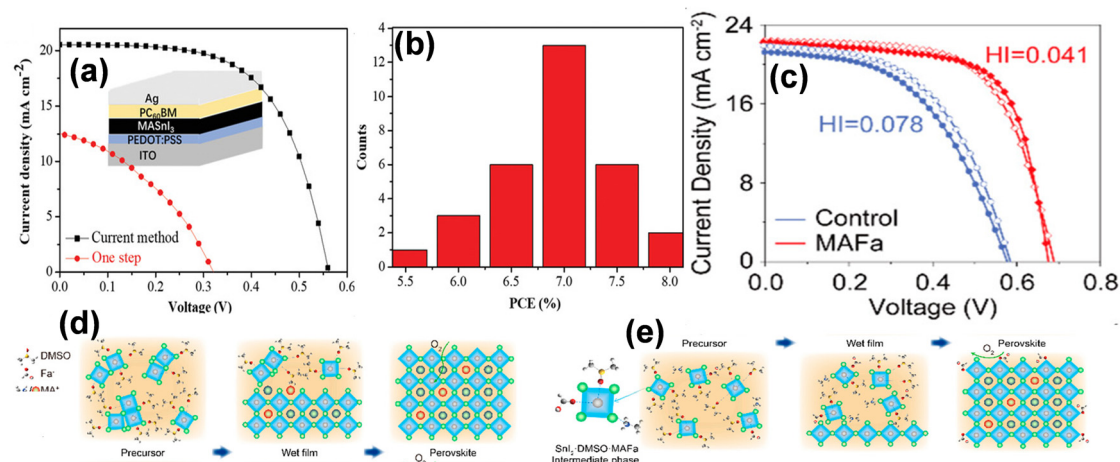
Fig. 4 (a) and (b) *J*−*V* curves and histograms of PCEs for 30 devices of MASnI$_3$ films, respectively. Reproduced with permission from ref. 54, copyright 2020, Wiley. (c) *J*−*V* curves of the control and MAFa-containing TPSCs. (d) and (e) Schematic of the crystallization process of the control and MAFa-derived perovskite films. Reproduced with permission from ref. 134, copyright 2023, ACS.

An extremely stable lead-free PSC was developed by fabricating high-quality FA$_{0.75}$MA$_{0.25}$SnI$_3$ films. This was achieved using the ionic liquid methylamine formate (MAFA), which stabilized the intermediate adduct. It effectively controlled the reaction rate of ammonium salts and SnI$_2$, in turn modulating Sn perovskite crystallization and preventing the formation of SnI$_2$ clusters, as shown in Fig. 4d and e. Thus, the PCE of the MAFA-derived perovskite films remarkably reached over 10% (Fig. 4c).[134] In further developments, Zhao and coworkers altered the composition of a perovskite material to achieve high performance. According to the calculated tolerance factor, the organic cations (MA/FA) and halide anions (I/Br) were varied in the perovskite structure to optimize the band structure and crystallinity of the MA$_{1−y}$-FA$_y$SnI$_{3−x}$Br$_x$ perovskite. It was observed that MA$_{0.4−02}$FA$_{0.6−0.8}$SnI$_{3−x}$Br$_x$ exhibited a suitable bandgap, high surface, and reduced voids with an increase in the Br ratio, and MA$_{0.3}$FA$_{0.7}$SnI$_{2.4}$Br$_{0.6}$ was found to be the optimal composition for device application.[135]

7.1.3. FASnI$_3$. FASnI$_3$ poses as a special candidate for Sn-based perovskites, which consists of only one stable α-phase. FASnI$_3$ is mainly present in two different crystal forms either cubic or orthorhombic. Cubic FASnI$_3$ has a lattice parameter of approximately 6.3290(9) Å and is very stable under atmospheric conditions. It possesses a band gap of nearly 1.4 eV, which is wider compared to MASnI$_3$ but relatively narrower than MAPbI$_3$. However, its band gap can be altered by employing numerous combinations of halogens and cations.[95] The band gaps of FASnBr$_3$ and FA$_{0.75}$MA$_{0.25}$SnI$_3$ are 2.4 eV and 1.33 eV, respectively.[136,137] The initial study on FASnI$_3$-based PSCs reported a modest PCE value of 2.1%.[138] Feng Yan and group introduced ammonium hypophosphite (NH$_4$H$_2$PO$_2$) in the FASnI$_3$ perovskite to enhance its stability by suppressing the oxidation of Sn^{2+}, assisting the growth of the perovskite grains. Additionally, CuSCN was applied as a hole transporting material (HTL) in the devices due to its high charge mobility and good energetic alignment with FASnI$_3$, as schematically presented in Fig. 5a.[139] The photovoltaic devices showed a significant enhancement in PCE, reaching up to 7.3% together with a *J*$_{sc}$ value of

19.39 mA cm^{-2} and fill factor (FF) of 68.8% (Fig. 5b). The PCE statistics of the FASnI$_3$ PSCs prepared were represented with different amounts of AHP (Fig. 5c).[139] High-efficiency Sn-based PSCs predominantly incorporate FASnI$_3$, which is attributed to its greater stability relative to MASnI$_3$. M. Chen introduced a large divalent organic ligand into FASnI$_3$ thin films to achieve high efficiency. As shown in Fig. 5d and e, 4AMP impacted the growth of the FASnI$_3$ grains in the polycrystalline thin film through strong functionalization of its external surface and internal interface and FASnI$_3$ was completely encapsulated *in situ* as the amount of 4MP increased. It improved the stability of the thin-film structure by inhibiting O$_2$/H$_2$O ingression into the bulk. Thus, the 4AMP-functionalized FASnI$_3$ perovskite thin film PSC device produced a remarkable PCE of 10.9% with a 500 h operational stability (Fig. 5f).[140]

To date, numerous studies have been conducted on Sn-based perovskite solar cells (PSCs). Table 1 summarizes the photovoltaic parameters observed across these investigations. The favored use of the FA cation can be attributed to the higher formation energies of Sn vacancies in FASnI$_3$, and thus a lower hole density relative to MASnI$_3$. Lin *et al.* demonstrated a new strategy to restrict Sn degradation under ambient conditions by adding the bidentate ligand 8-hydroquinone in inverted FASnI$_3$ PSCs. The 8-HQ ligand can coordinate with the Sn^{2+} sites *via* its nitrogen and oxygen atoms and inhibit the conversion of Sn^{2+} to Sn^{4+}. Thus, the film quality and stability of the PSC improved effectively with reduced defect states, subsequently enhancing its photovoltaic performance. Fig. 5g and h represent the device structure based on 8-HQ coordinated FASnI$_3$, and the corresponding devices showed an excellent PCE of 7.15% with high *J*$_{sc}$ and *V*$_{oc}$.[141] Meng *et al.* reproduced an improved FASnI$_3$ PSC by introducing liquid formic acid as a reducing solvent, resulting in the production of the FASnI$_3$ perovskite film and leading to an efficiency of over 10.37% under AM1.5G illumination (Fig. 5i).[142]

Li *et al.* developed a highly oriented 2D halide perovskite film for stable lead-free PSCs. Additive phenyl ethylammonium chloride (PEACl) was utilized on FASnI$_3$ perovskite to grow the FASnI$_3$:PEACl film in a highly crystalline 2D-phase, as presented
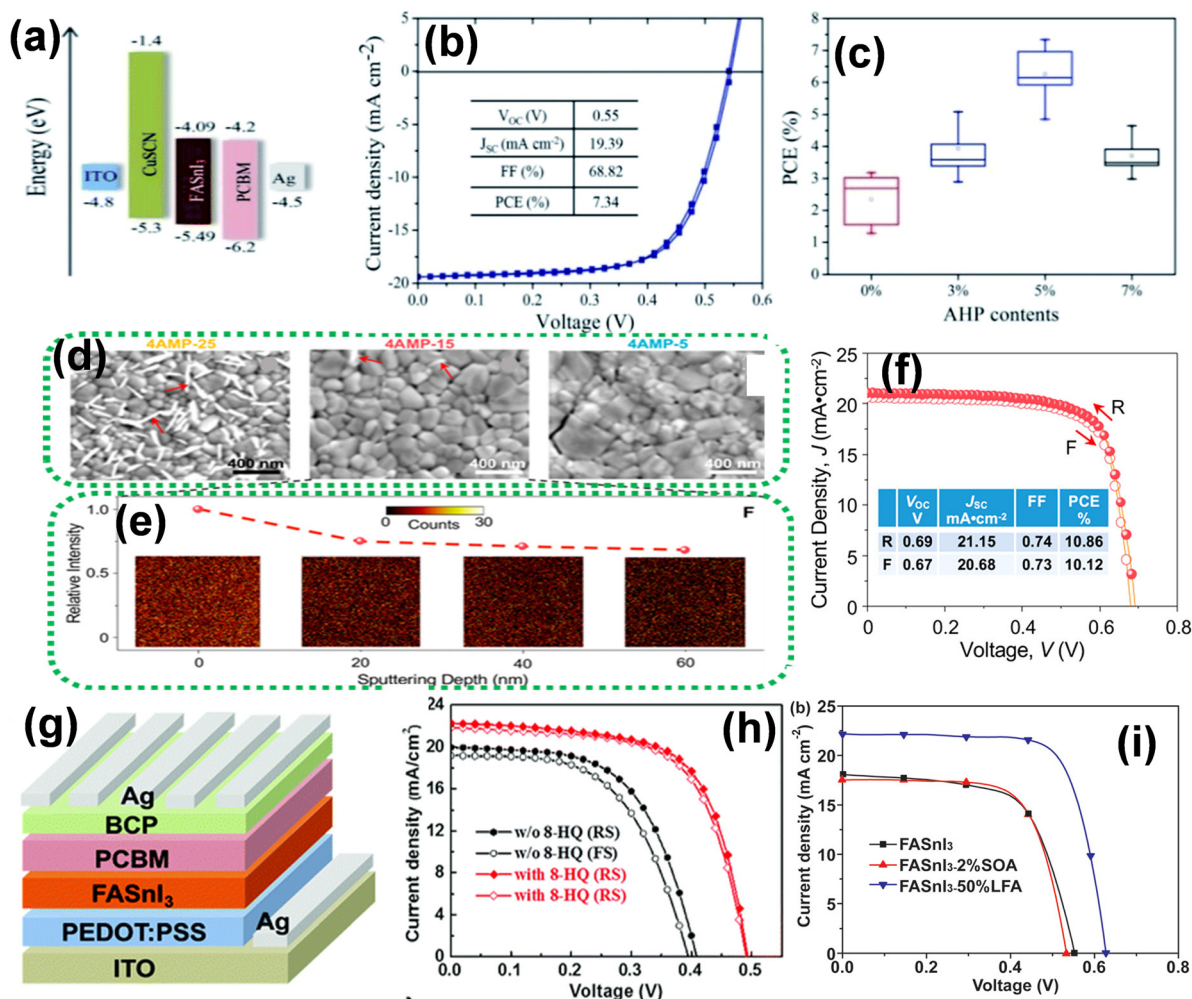
Fig. 5 (a) Band structure, (b) $J–V$ curve of FASnI$_3$-based PSCs, and (c) PCE statistics for FASnI$_3$-based PSCs with different amounts of AHP. Reproduced with permission from ref. 139, copyright 2019, RSC. (d) SEM images of the perovskite thin films of 4AMP-25, 4AMP-15, and 4AMP-5, (e) TOF-SIMS intensity as a function of sputtering depth in the 4AMP-15 thin film, and (f) $J–V$ curve of 4AMP-15-based device. Reproduced with permission from ref. 140, copyright 2020, ACS. (g) PSC device structure based on FASnI$_3$ and (h) $J–V$ curves of the best devices without and with 8-HQ. Reproduced with permission from ref. 141, copyright 2020, RSC. (i) $J–V$ curves of FASnI$_3$-based devices. Reproduced with permission from ref. 142, copyright 2020, ACS.

in Fig. 6a. It was revealed that the annealing of Sn perovskite, facilitated by PEACl, promoted the formation of a vertically oriented, highly ordered 2D crystal structure. FASnI$_3$:PEACl PSCs were fabricated with NiO$_x$ or PEDOT:PSS as HTLs. The PEACl additive in the PSC device functioned as a surface barrier layer, effectively protecting the Sn layer from the oxidation process at room temperature. This resulted in an improvement in device efficiency, with the PCE exceeding 9% (Fig. 6b and c).[156] In a similar strategy, X. Xui and coworkers constructed a three-dimensional (3D) perovskite film by applying a mixed-cation strategy with doping of hydrophobic additive. Fig. 6d and e present the device structure of the PSCs and $J–V$ curves of the PSCs with different amounts of mol% for DPPAI under simulation, respectively. Sn-based halide perovskites were formed using FA and 3,3-diphenylpropylammonium (DPPA) as mixed cations in different ratios. The optimal DPPA$_{0.02}$FA$_{0.98}$SnI$_3$-based perovskite achieved the highest PCE of 6.75% with increased device performance across all parameters. Notably, the trace-doping of

these cations enhanced the morphology and crystallinity of the perovskite film, leading to long-term stability and suppression of non-radiative recombination, resulting in a high PCE.[157]

FASnI$_3$-based perovskites are similar to lead-based perovskites but have poor crystallinity. Thus, to resolve this problem, Zhu et al. developed a one-step-spin coating method to form FASnI$_3$ films using an antisolvent. The spin coating and annealing of FASnI$_3$ (Fig. 6f and g) were performed in the presence of N-trimethylthiourea (3T). 3T served as a Lewis base as well as an H-bond donor to provide uniform morphology and high stability to the perovskite film. The photoluminescence analysis revealed that the 3T-treated films exhibited a longer carrier lifetime of 123 ns, surpassing other reported perovskites and reducing the charge recombination effectively. Consequently, the PSC device performance was highly improved, displaying a certified PCE of 14.0% (Fig. 6h).[149] Later, Zuraw et al. proposed a tin powder–carboxylic acid-assisted synthesis to prepare pure and stable SnI$_2$ for developing lead-free perovskites. In this

Table 1 Pb-free PSC performance parameters

S. no.	Light absorber	Device structure	Synthetic method	Band gap (eV)	Carrier lifetime (ns)	V_{oc} (V)	J_{sc} (mA cm^{-2})	FF%	PCE (%)	Ref.
1.	FASnI3	PET/IZO/PEDOT:PSS/FASI3/C60/BCP/Ag.	One-step spin coating	—	—	0.59	21.60	66.5	8.35	143
2.	PEA0.2FA0.8SnI3	ITO/HTLs/PEA0.2FA0.8SnI3/ICBA/BCP/Ag	One-step spin coating	1.42	10.3	0.60 ± 0.06	20.7 ± 0.4	51.8 ± 3.6	6.3 ± 0.6	144
3.	FASnI3	ITO-PEDOT:PSS-perovskite/C60/BCP/Ag.	One-step spin coating	1.43	21.2	0.84	23.19	72	14.5	145
4.	FASnI3	ITO/PEDOT:PSS/perovskite/PCBM/BCP/Ag	Antisolvent method	1.43	27	0.85	20.50	71	12.45	56
5.	Cs2SnI6	FTOTiO2-Cs2SnI6/P3HT/Ag	Solution processing method	2.14	—	0.25	7.41	24	0.47	130
6.	FASnI3	ITO/PEPOT:PSS-FASnI3/PCBM/BCP/Ag	Antisolvent method	1.4	—	0.31	17.64	41	2.28	146
7.	FA0.8PEA0.2SnI2.8Br0.2	ITO/PEDOT:PSS-Sn-PVK/ICBA/BCP/Ag	One-step spin coating	1.23	—	0.86	19.7	73	12.9	53
8.	FASnI3	ITO/PEPOT:PSS-FASnI3/PCBM/PEI/Ag	—	1.41	—	0.64	13.36	56	5.51	147
9.	FA0.75MA0.25SnI3	ITO/PEDOT:PSS-FA0.75MA0.25SnI3/C60/BCP/Al	One-step spin coating	1.34	5.07–6.22	0.69	22.4	63	10.1	134
10.	CsSnI3	ITO/PCBM/CsSnI3/CFTS/Se	—	—	—	0.87	33.99	83.4	24.73	131
11.	FASnI3	FTO/WO3/FASnI3/CZGS/MoOx:Au	—	—	—	0.75	32.84	46	17.10	148
12.	FASnI3	ITO/CuI/CsSnI3/C60/BCP/Al	Two-step spin coating	1.4	123	0.92	20.3	77	14.0	149
13.	FASnI3	ITO/PEDOT:PSS//C60/BCP/Ag	One-step spin coating	1.42	12.4	0.49	22.24	65.19	7.15	142
14.	PEA0.15FA0.85SnI3	PEDOT:PSS	Antisolvent method	1.39	—	0.47	22.7	67.8	7.3	60
15.	MASnIBr2	FTO/cTiO2/mTiO2/MASnIBr2/spiro-OMETAD/Au	One-step spin coating	1.75	—	0.58	11.09	49	3.2	133
16.	PTN-Br + SnF2	ITO/PEDOT:PSS-FASnI3/C60/BCP/Ag	Antisolvent method	1.35	—	0.57	20.66	67.40	7.94	150
17.	GeI2 + SnF2	ITO/PEDOT:PSS/PEA0.08 FA0.92Sn1−xGexI3/C60-BCP/Ag/Au	Two-step sequential coating	1.45	—	0.46	21.92	73.0	7.45	151
18.	RbCl + SnF2	ITO/PEDOT:PSS/FA1−xRbxSnI3-PCBM/BCP/Ag	Antisolvent method	1.34	—	0.487	20.04	60.4	5.89	152
19.	TBAI + SnF2	ITO/PEDOT:PSS-FASnI3/PCBM/BCP/Ag	One-step spin coating	1.34	—	0.51	19.7	69.6	7.0	153
20.	PDI2 + SnF2	ITO/PEDOT:PSS-FASnI3C60/BCP/Ag	One-step sequential coating	1.37	127 ns	0.69	21.85	75.1	11.39	154
21.	NH4SCN + SnF2	ITO/PEDOT:PSS/PEAxFA1−xSnI3-ICBA/BCP/Ag	Antisolvent method	1.39	—	0.94	17.4	75	12.4	155
22.	FASnI3	FASnI3:PEACl	Antisolvent method	—	—	0.59	22.06	69	9.1	156
23.	FASnI3	ITO/PEDOT:PSSDPPA,FA1−xSnI3-C60/BCP/Ag	Antisolvent method	—	2.16	0.45	14.47	63.03	4.12	157
24.	FASnI3	glass//ITO/PEDOT:PSS/FASnI3/PCBM-BCP/Ag	One-step spin coating	—	1.4	0.49	22.24	65.19	7.15	141
25.	MASnI3	ITO/PEDOT:PSS/MASnI3/PC61BM/BCP-Ag	Multi-step sequential coating	—	—	0.57	20.68	66	7.78	54
26.	(FA,MA)SnI3	Au/spiroOMeTAD/FAxMA1−xSnI3/TiO2/FTO	One-step spin coating	1.35–1.43	7.76–6.72	0.58	19.80	46.65	5.37	132
27.	FASnI3	ITO/CuSCN/FASnI3-PCBM/Ag	Two-step sequential spin coating	1.4	—	0.55	19.39	86.8	7.3	139
28.	Ag3Bi6−2xsx	FTO/TiO2/Ag3Bi6−2xsx/spiro-OMeTAD/Au	—	1.65–1.85	110	0.57	14.60	65	5.44	158
29.	AgBi2I7	FTO/TiO2/AgBi2I7/spiro-OMeTAD/Au	Two-step sequential coating	1.89	—	0.54	2.81	46	0.69	159
30.	MA3Sb2I9	FTO/c-TiO2/LFPSCS-6/P3HT/carbon	One-step spin coating	2.2	—	0.55	3.70	48	0.91	160
31.	CsBi3I10	ITO/NiOx/perovskite layer/PC61BM/BCP/Ag.	Ligand-assisted reprecipitation	1.77	—	0.79	4.2	69	2.30	161
32.	Cs3Bi2I9	ITO/NiOx/perovskite layer/PC61BM/BCP/Ag.	Ligand-assisted reprecipitation	2.05	—	0.62	2.4	47	0.70	161
33.	Rb3Sb2I9	FTO/c-TiO2,|Rb3Sb2I9-poly-TPD|Au	Two-step deposition	2.24	—	0.61	5.54	40	1.35	162
34.	(CH3NH3)3Bi2I9	ITO/PEDOT:PSS-Sn/C60/BCP/Ag	Antisolvent method	2.1	—	0.51	0.94	61	0.31	163
35.	(CH3NH3)3Bi2I9	FTO/c-TiO2-Meso-TiO2/P3HT	One-step spin coating	2.1	—	0.87	2.70	69	1.62	164
36.	AgBi2I-DMF	—	Two-step deposition	0.54	46	0.54	2.81	46	0.69	159
37.	AgBi2I7-DMF:MeOH	—	Two-step deposition	0.65	48	0.65	3.07	48	0.96	159
38.	AgBi2I-DMF	—	Two-step deposition	0.54	46	0.54	2.81	46	0.69	159
39.	CsBi3I10	ITO/PEDOT:PSS/CBI/BCP/C60/BCP/Ag.	Two-step spin coating	1.78	1.92 ns	0.67	2.46	49	0.80	165
40.	(CH3NH3)3Bi2I9	FTO/CLTiO2/mTiO2/MBI/spiro-MEOTAD/Au	Two-step deposition	2.2	—	0.87	1.6	34	0.41	166
41.	(CH3NH3)3Bi2I9	F/SnO2/FTO/TiO2	Chemical vapour deposition	2.30	—	0.40	0.11	36	0.016	167
42.	(CH3NH3)3Bi2I9	—	Antisolvent method	2.0	—	0.59	0.5	57	0.17	168
43.	(FA)3Bi2I9	FTO/C-TiO2-meso-TiO2/perovskite/spiro/Au	One-step spin coating	2.19	—	0.48	0.11	46	0.022	169
Sb-based										
44.	Cs4CuSb2Cl12	FTO/WS2/Cs4CuSb2Cl12/CuSbS2/Ni	—	1.6	—	1.17	23.75	83	23.10	73
45.	(CH3NH3)3Sb2I9	—	Antisolvent method	1.55	—	0.74	1.48	52	0.57	72

Table 1 (continued)

S. no.	Light absorber	Device structure	Synthetic method	Band gap (eV)	Carrier lifetime (ns)	V_{oc} (V)	J_{sc} (mA cm^{-2})	FF%	PCE (%)	Ref.
46.	Rb$_3$Sb$_2$I$_9$	ITO/cTiO$_2$/mpTiO$_2$/Rb$_3$Sb$_2$Br$_{9-x}$I$_x$/spiro-OMeTAD/Au.	Antisolvent vapor diffusion crystallization	2.02	—	0.55	4.25	59.5	1.37	170
47.	Rb$_3$Sb$_2$I$_9$	—	One-step spin coating	2.24	—	0.55	2.11	57	0.66	106
48.	(CH$_3$NH$_3$)$_3$Sb$_2$I$_9$	FTO/CL-TiO$_2$/m-TiO$_2$/MASbI-HTM/Au	Two-step deposition	2.1	—	0.69	0.39	—	0.10	171
49.	(CH$_3$NH$_3$)$_3$Sb$_2$I$_9$	FTO/CL-TiO$_2$/m-TiO$_2$/MASbI/HTM/Au	Two-step deposition	2.1	—	0.74	1.40	—	0.54	171
50.	(NH$_4$)$_3$Sb$_2$I$_9$	FTO/CLTiO$_2$/mTiO$_2$/(NH$_4$)$_3$Sb$_2$I$_9$-HTM/Au	Two-step deposition	2.05	0.47	0.94	—	—	0.42	172
Ge-based										
51.	NiO$_x$/FASn$_{0.9}$Ge$_{0.1}$I$_3$	PEDOT:PSS HTL	One-step spin coating	1.4	—	0.69	21.3	71	10.43	173
52.	Ge:EDA$_{0.01}$FA$_{0.98}$SnI$_3$	PEDOT:PSS	Antisolvent method	1.39	—	0.51	21.39	63	6.8	60
53.	CsSnGeI$_3$	Au/spiro-OMeTAD/CsSn$_{0.5}$Ge$_{0.5}$I$_3$/spiro-OMeTAD/Au	Solid-state synthesis	1.5	10.92	0.63	18.61	60	7.11	174
54.	CsSnGeI$_3$	FTO/PCBM/(IL1)/CsSn$_{0.5}$Ge$_{0.5}$I$_3$/(IL2)/spiro-OMeTAD/Au		1.5	—	1.17	25.80	80.33	24.20	175
55.	CsSn$_{0.5}$Ge$_{0.5}$I$_3$	Au/spiro OMeTAD/PCBM/FTO	Solid-state synthesis	1.50	10.92	0.63	16.61	60	7.11	174
Double lead-free perovskites										
56.	Cs$_2$Ag$_x$Na$_{1-x}$Bi$_{1-y}$In$_y$Cl$_6$	Cs$_2$NaBiI$_6$ (CNBI)	Room temperature synthesis	—	—	0.67	2.38	75	23.13	176
57.	Cs$_2$AgBiBr$_6$	FTO/bl&mpTiO$_2$/Cs$_2$AgBiBr$_6$/HSL/Au	One-step spin coating	—	10^{-6} s	1.59	3.73	74	2.92	177
58.	FA$_4$GeSbCl$_{12}$	FTO/TiO$_2$/FA$_4$GeSbCl$_{12}$/Cu$_2$O/Au	—	1.3	—	0.76	34.52	85.1	22.25	178

approach, Sn nanoparticles were inherently grafted with carboxylic acid *via* an *in situ* reaction. The utilization of carboxylic acid is not only advantageous for the formation of SnI$_2$ but also develops a stable lead-free perovskite by mitigating Sn oxidation. It established the fabrication of a reproducible large-area (1 cm^2) flexible perovskite solar cell, which exhibited a remarkable PCE of 8.35% with an improved open-circuit voltage.[143] Further, Gao *et al.* reported an improved hybrid tin halide-based perovskite for solar cell applications by using dipropyl sulfide (DPS) as an additive. Their study demonstrated that the DPS molecules effectively coordinated with Sn molecules to increase the stability of the Sn^{2+} ions, facilitating the formation of an intermediate complex. This stabilization hindered the crystallization and oxidation of the prepared films. Thus, the device showed an enhanced PCE from 11.0% to 12.9%, accompanied by reduced charge recombination and a small leakage current. Additionally, the device stability was significantly enhanced. It is known that tin-based perovskites show the highest performance as lead-free PSCs. Sn-based halide perovskites, typically FASnI$_3$, are mostly similar to their lead-based substituents in terms of optoelectronic properties but struggle with dissimilar crystallization kinetics.[183]

Further, Fakharuddin and coworkers proposed an interesting work with MXene-embedded PEDOT:PSS as HTL for enhancing the performance of PSCs. Due to MXene-PEDOT:PSS HTL combination, a modified perovskite film was obtained with low pinhole density and a uniform contact potential difference, leading to a high PCE. The modified PSC delivered a PCE of 8.35%, which was comparatively higher than that of its pristine counterpart (7.35%) (Fig. 6i).[144] In another work, Kuan *et al.* explored the incorporation of acetamidinium and rubidium (Rb) as co-cations in varying proportions in the FASnI$_3$ perovskite structure. The observation indicated that AC effectively passivated the defects on the surface of the film, at its interface with the substrate, and within the bulk material, while Rb primarily mitigated the interface defects between the PEDOT:PSS and perovskite layer, as shown in Fig. 6j. It improved phase stability, due to which non-radiative recombination was effectively inhibited and the charge mobility was drastically enhanced. The films prepared with these co-cations demonstrated the optimal performance at 10% AC (E1AC10) and 3% Rb (E1AC10Rb$_3$), as presented in Fig. 6k. Consequently, the E1AC10Rb$_3$ device attained a PCE of 14.5% and demonstrated exceptional stability, maintaining its performance over 3000 h.[145] Recently, Hongqiang Wang and co-workers enhanced the efficiency of low-dimensional and 2D/3D Sn-PSCs from 7.97% to 12.45% by incorporating a multifunctional molecule such as D-homoserine lactone hydrochloride. The corresponding device is presented in Fig. 6l together with its band gap energy and efficiency results in Fig. 6m and n, respectively. Their study revealed that D-HLH forms H-bonds with FA$^+$ and I$^-$ ions and binds with Sn^{2+} through Sn–O bonds. This improved crystallization process enhanced both the efficiency and stability of the resulting PSC device.[56] Herrera *et al.* conducted a simulation-based (Fig. 6o) study on the photovoltaic performance of FASnI$_3$-based PSCs with a regular device architecture
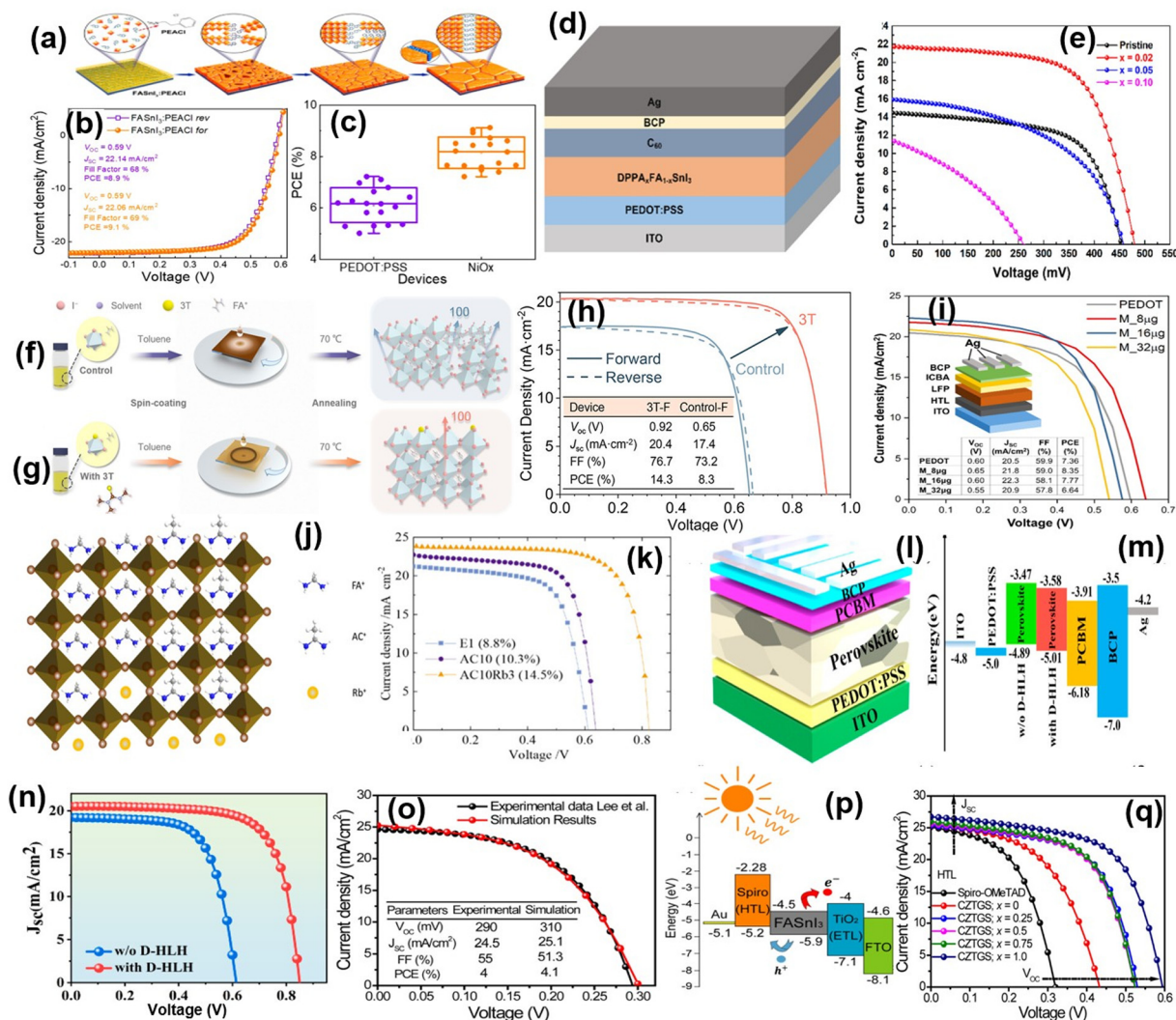
Fig. 6 (a) Schematic of the crystallization process of $FASnI_3$ and $FASnI_3$:PEACl films. (b) $J-V$ curves and (c) IPCE spectra of $FASnI_3$:PEACl-based PSCs. Reproduced with permission from ref. 156, copyright 2020, ACS. (d) Device structure model of the PSCs. (e) $J-V$ curves of PSCs with different DPPAI amounts at different mol%. Reproduced with permission from ref. 157, copyright 2020, ACS. (f) and (g) Schematic of the crystallization process of $FASnI_3$ films with and without N-trimethylthiourea (3T), respectively and (h) $J-V$ curves of devices with or without 3T. Reproduced with permission from ref. 149, copyright 2022, ACS. (i) $J-V$ curves of MXene-embedded PEDOT:PSS-based PSC devices. Reproduced with permission from ref. 144, copyright 2024, ACS. (j) and (k) Crystalline structure and characteristic $J-V$ curves for $E1AC_{10}Rb_3$ film and PSC device, respectively. Reproduced with permission from ref. 145, copyright 2024, ACS. (l) Device architecture of tin PSCs. (m) Energy level diagram of tin PSCs. (n) $J-V$ curves of tin PSCs with and without D-HLH. Reproduced with permission from ref. 56, copyright 2024, ACS. (o) Comparison of $J-V$ characteristics between simulation and experimental results, (p) flat band energy diagram, and (q) $J-V$ curves of PSCs employing CZTGS with different ratios. Reproduced with permission from ref. 148, copyright 2024, ACS.

(Fig. 6p). They also incorporated a typical organic HTL material, spiro-OMeTAD, to evaluate its impact on the device behaviour. The theoretical investigation suggested that the PSC showed an inspiring PCE of 17.1% by using an MoOx:Au composite in place of the Au back contact, which optimized the alignment of the energy levels at different heterojunctions and led to a high performance (Fig. 6q).[148]

7.2. Ge-based perovskite solar cells ($AGeX_3$)

Ge-based perovskites exhibit low acute toxicity and share several favourable properties with lead-based perovskites, though they are not as closely matched in characteristics as their Sn analogs.[184] Pb^{2+} and Ge^{2+} have almost same similar

coordination types, electronic configurations, and crystal structures, and therefore Ge seems to be an alternative candidate for Pb, which can also satisfy the requirements of both charge balance and coordination. Germanium perovskites provide a safer, less toxic option and demonstrate some promising photovoltaic qualities but they typically exhibit lower stability and performance compared to lead- and tin-based alternatives. A comparison of the unit cells of cubic metal halide perovskites $CsGeX_3$ (X = I, Br, Cl) with Pb-based complexes $CsPbX_3$ is presented in Fig. 7a.[126] This limits their current applicability in high-efficiency solar cells, although ongoing research seeks to improve their optoelectronic properties and stability to make them more competitive. The structural and electrical properties
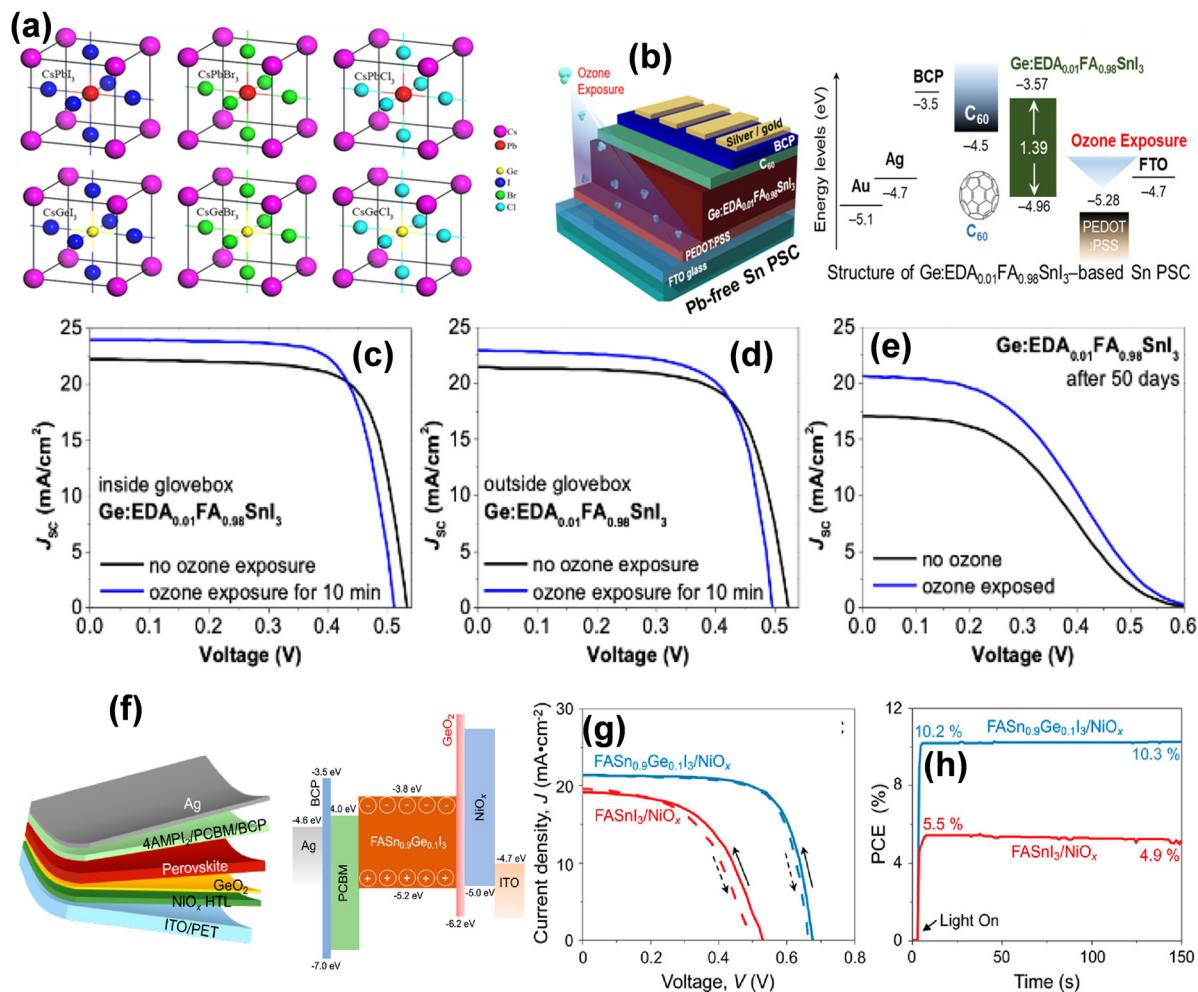
Fig. 7 (a) Representation of unit cells of $CsBX_3$ (B = Ge and Sn) composed of different halide anions. Reproduced with permission from ref. 126, copyright 2017, Nature Scientific Reports. (b) $Ge:EDA_{0.01}FA_{0.98}SnI_3$-based PSC device and corresponding energy-level diagrams. (c)–(e) J–V curves of $Ge:EDA_{0.01}FA_{0.98}SnI_3$ PSCs with and without ozone exposure, measured inside the GB, outside the GB, and after 50 days in air, respectively. Reproduced with permission from ref. 60, copyright 2020, ACS. (f) Schematic of the adopted architecture of the f-PSC and its corresponding energy-level diagram. (g) J–V responses of "champion" f-PSC devices. (h) Stable output of "champion" f-PSC devices. Reproduced with permission from ref. 173, copyright 2022, ACS.

of $MAGeX_3$ are mostly matched to $MAPbX_3$, making it a suitable Pb substitute in halide perovskites. Current research in perovskite solar cells indicates that Ge-based perovskites exhibit lower efficiency than Sn-based perovskites. Thus, realizing high-efficiency solar cells with Ge-based perovskites remain a significant challenge. Nonetheless, theoretical investigations indicated that Ge-containing perovskites possess excellent optoelectronic properties suitable for solar applications. Researchers continue to explore ways to harness these properties, with a focus on enhancing the stability and optimizing the performance of Ge-based perovskites to make more viable in photovoltaic technologies.[184–186] Qian *et al.* first performed DFT calculations on the $CsGeI_3$ inorganic halide perovskite to examine its electronic structure and optical properties and compared it with the $CH_3NH_3PbI_3$ perovskite. Interestingly, the bandgap of $CsGeI_3$ and $CH_3NH_3PbI_3$ was found to be 1.51 and 1.55 eV, respectively, and their charge mass transport ratio

is also nearly matched, suggesting that Ge is a good replacement for the fabrication of Pb-free solar cells. This is also evident from the calculated PCE value of 27.9% and 26.7% for $CsGeI_3$ and $CH_3NH_3PbI_3$, respectively.[186]

However, Ge is a rare and costly metal; thus, Ge is preferably mixed with other cations such as Sn to fabricated mixed cation-based lead-free PSCs. Considering this, Chen *et al.* introduced the $CsSn_{0.5}Ge_{0.5}I_3$ perovskite composition by alloying Ge(II) with $CsSnI_3$. The $CsSn_{0.5}Ge_{0.5}I_3$ perovskite solid solution exhibited remarkable stability, with less than a 10% decline in efficiency over 500 h in the corresponding PSCs. It also possesses decent absorption in the visible region with an optical band gap of 1.50 eV, which lies between the bandgaps of its pure form perovskites. The Ge/Sn-mixed perovskite material was utilized as a light absorber in perovskite solar cells (PSCs) and a promising PCE of up to 7.11% was achieved.[174] Ng *et al.* described the role of additives in new Sn/Ge-based perovskites

on their photovoltaic performance. The $FA_{0.75}MA_{0.25}Sn_{1-x}Ge_xI_3$ perovskite, depicted as $FMS_{1-x}G_xI$, was prepared and further coated with SnF_2 and GeI_2 additives. The presence of SnF_2 retarded Sn^{2+} degradation into Sn^{4+} and reduce the Sn vacancies in the PSC. Alternatively, GeI_2 (5 mol%) drastically reduced the trap density, resulting in a longer charge lifetime and diffusion coupled with excellent charge mobility. Thus, the Ge-doped perovskite attained a longer lifetime of excitons, higher charge mobility, and longer charge diffusion, which were significantly higher than that of the pristine perovskite, achieving a high PCE of 7.9%. This work demonstrated that modification of the optoelectronic properties *via* additives opens a new platform for designing Ge-based PSCs with high performance.[187]

Later, Nam *et al.* introduced a cheaper, cost-effective, and effective ozone exposure method for PEDOT:PSS to fabricate Ge-based perovskites to improve the device performance.[60] They fabricated $Ge:EDA_{0.01}FA_{0.98}SnI_3$-based PSCs in the configurational structure presented in the schematic illustration in Fig. 7b along with its energy level diagram. The ozone-exposed PEDOT:PSS-based devices fabricated using the synthesized perovskite demonstrated comparable power conversion efficiencies (PCEs) both outside and inside their grain boundaries, which was attributed to their enhanced stability (Fig. 7c). Specifically, the ozone-treated PEDOT:PSS utilized in the $Ge:EDA_{0.01}FA_{0.98}SnI_3$-based tin perovskite solar cells (Sn-PSCs) achieved an increased PCE of 8.1%, which was higher than that of the pristine perovskite (Fig. 7d). It was revealed that the ozone exposure significantly lowered the Fermi level of PEDOT:PSS and tuned their energy levels, improving the hole mobility and reducing the trap density for the device to achieve a significantly higher performance. Furthermore, the $Ge:EDA_{0.01}FA_{0.98}SnI_3$-based Sn-PSCs maintained a significant PCE performance even after 50 days of air exposure (Fig. 7e). The stability differences between the ozone-exposed and untreated PEDOT:PSS-based Sn-PSCs were negligible, which indicated that ozone exposure did not adversely impact the stability of the perovskites.

Recently, Chen *et al.* reported another method for the fabrication of flexible Ge-doped lead-free PSCs using an innovative compositional and interfacial engineering approach, producing the highest efficiency of 10.43% to date. Their work revealed that the *in situ* growth of the GeO_2 layers occurred at the interface between the Sn-based perovskite film and NiO_x HTL to form a new $FASn_{0.9}Ge_{0.1}I_3$ layer. The role of Ge in the $FASnI_3$ perovskite (MHP) is to stabilize the Sn^{2+} site in the MHP film having NiO_x as the HTL. Thin films of $FASnI_3$ and $FASn_{0.9}Ge_{0.1}I_3$ were integrated into flexible perovskite solar cells (f-PSCs), and their photo-efficiency, operational stability, and mechanical strength were assessed. The adopted architecture of the f-PSC is depicted in Fig. 7f, with the corresponding energy-level diagram. In this configuration, a thin film of perovskite is positioned between two different HTL electron transport layers (ETL). This led to no apparent photocurrent leakage and restricted interfacial charge recombination, which is evident from the high V_{oc} and FF values. Thus, the PSC device achieved an all-time record efficiency of 10.43% together with a

high V_{oc} and J_{sc} of 0.69 V and 21.3 mA cm^{-2}, respectively, and a fill factor (FF) of 0.71 (Fig. 7g). This represents the highest reported PCE for a lead-free f-PSC to date. Fig. 7h further shows the stable PCE output of 10.3% at the maximum power point, consistent with the *J–V*-derived PCE, affirming the reduced hysteresis behavior of the device.[173]

7.3. Bi-based perovskite solar cells ($ABiX_3$)

Bi and its compounds have advantages and disadvantages. Many bismuth compounds are applicable for medicinal purposes, while their chronic intake can be harmful and result in encephalopathy and renal failure. However, low concentrations of bismuth (1 to 100 mM) are non-toxic to human health. The Bi^{3+} ion possess an identical ionic radius and electronic configuration as Pb, and thus has potential for Pb substitution. Bi is a stable element under ambient conditions and almost non-toxic compared to the Ge and Sn elements. Bi forms trivalent ions and the perovskite structure can be obtained by replacing three Pb^{2+} with two Bi^{3+} ions. Thus, trivalent Bi^{3+}-based perovskites have a structure of $A_3Bi_2X_9$ with generally an octahedral-coordinated structure, where A is occupied by a cation such as Cs^+ and MA^+, while the X position is occupied by a halide ion such as Br^- and I^-. The first $Cs_3Bi_2I_9$ PSC was reported with a PCE of over 1%. After that, several bismuth-based perovskite solar cells have been reported with an improved PCE. Jain *et al.* utilized a sustainable approach to fabricate lead-free, Bi-based $(CH_3NH_3)_3Bi_2I_9$ (MBI) perovskite films by applying a non-toxic methyl acetate solution. The MBI devices were fabricated with two different HTLs, spiro-OMeTAD and P3HT, which produced an efficiency of 1.12% and 1.62%, respectively. The photovoltaic performance of the PSCs and the energy band level diagram and device architecture are displayed in Fig. 8a. Fig. 8b represents the *J–V* characteristics of the respective solar cells.[164] Our group prepared an improved hybrid bismuth-based lead-free perovskite ($AgBi_2I_7$) through the solvent engineering technique and utilized it as the light absorber layer in PSCs. Two different solvents, DMF and MeOH, were employed in an optimum ratio to improve the photovoltaic efficiency. This work revealed that the optimal combination of the solvent system reduced the band gap to 1.89 eV, leading to a PCE value of 0.96% for the Bi-based solar cells (Fig. 8c). However, the theoretical investigation calculated a maximum efficiency of 13.26% using $AgBi_2I_7$ as a light absorber in PSCs.[159] Karim *et al.* demonstrated stable $Cs_2AgBiBr_6$-based PSCs by optimizing the thin-film fabrication conditions and presenting a buffer interfacial layer (BIL) at the perovskite/ETL interface. The introduction of BIL as a hole leakage barrier at the interface significantly improved the electrical contact at the interface, resulting in an enhanced device performance. This interfacial engineering approach led to a PCE of 0.80% with high reproducibility, which was substantially higher than that of the control PSC (0.38%).[165] In another work, our group introduced methyl acetate as an innovative solvent for preparing thin films of pristine perovskite materials. We demonstrated that the incorporation of Sn(IV) into the $MA_3Bi_2I_9$ lead-free perovskite structure resulted in the formation of $MA_3(Bi_{1-x}Sn_x)_3I_9$. Subsequently,
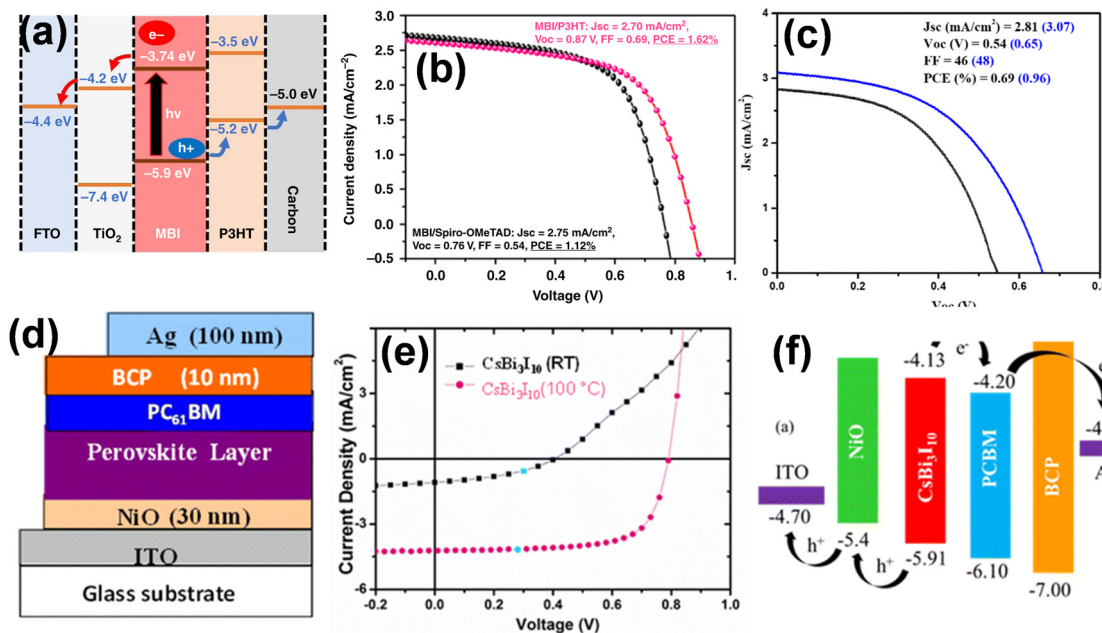
Fig. 8 (a) Optical band gap and (b) photovoltaic performance of MBI-based PSC devices. Reproduced with permission from ref. 164, copyright 2019, Springer Nature. (c) J–V curves of SBI-D and SBI-DM under 1 sun conditions. Reproduced with permission from ref. 159, copyright 2023, RSC. (d) Device architecture, (e) J–V measurements, and (f) energy level diagram of $CsBi_3I_{10}$-based devices (before and after annealing). Reproduced with permission from ref. 161, copyright 2023, RSC.

lead-free perovskite solar cell (LFPSC) devices were fabricated using pristine $MA_3Bi_2I_9$ and Sn(IV)-doped $MA_3(Bi_{1-x}Sn_x)_3I_9$ (where $x = 0$, 0.1, 0.2, 0.3, 0.4, and 0.5) as the light-absorbing layers. Theoretical studies of the LFPSC devices demonstrated a high PCE value of 12%, highlighting the significant potential of these materials for advancing LFPSC technologies.[160] For the first time, our group introduced a two-step deposition method for the fabrication of a device showing a good performance with 0.41% efficiency in comparison to the one-step deposition method for the fabrication of Pb-free PSCs.[166] Ahmad et al. from our group introduced a new light Bi-based absorber for lead-free perovskites [[(CH₃NH₃)₃-Bi₂Cl₉]ₙ in the form of a 1D-polymeric chain.[188] This perovskite exhibited non-toxic behavior and high stability with a remarkable open circuit voltage of 430 mV. However, the PCE of the device was found to be very low compared to another reported perovskite, which can be ascribed to its large bandgap of 2.85 eV. An efficient work was carried out by Vijaya et al. using the ligand-assisted re-precipitation approach (LARP) to produce two perovskites, $Cs_3Bi_2I_9$ and $CsBi_3I_{10}$, for photovoltaic application. This is one of the best methods to prepare low-cost and highly efficient perovskites under atmospheric conditions. Interestingly, the $CsBi_3I_{10}$-based PSC displayed a PCE value of 2.3% with an increase in fill factor (FF) by 69% as compared to that of the $Cs_3Bi_2I_9$-based device, showing a low efficiency of 0.7%. The device architecture, J–V curves and energy level diagram of the $CsBi_3I_{10}$-based device before and after annealing are shown in Fig. 8d–f, respectively.[161] Recently, Sekar et al. conducted a theoretical simulation of the PCE efficiency of Ag_3BiI_6-based solar cells using CeOx as the HTL. This investigation considered various factors such as different ETLs, absorber layers, and three different HTLs to tune their thicknesses and density and calculate high-performance solar

cells. Finally, the optimized planar Pb-free solar cells with Se/Te–Cu_2O HTL achieved a high PCE value of 17.77%.[158] This work emphasizes the fact that the efficiency of the proposed device can be calculated by theoretical investigation, which will be helpful for experimentalists to obtain highly efficient PSCs.

7.4. Sb-based perovskite solar cells

Sb-based PSCs have emerged as potential alternatives for Pb-based PSCs, offering a more cost-effective solution compared to their Sn-based counterparts. Antimony possesses a stable lone pair of $5s^2$ electrons, which contributes to its unique properties. This element is naturally found in environments associated with volcano and sea spray, with an average concentration in soil of approximately 0.48 ppm. Incorporating specific ions into the crystal lattice of Sb-based perovskites has been identified as a viable strategy to tune and enhance their optoelectronic properties, making them suitable for advanced photovoltaic applications.[189] Most of the human population is already exposed to low levels of antimony, which shares several characteristics with arsenic due to its position in the same group of the Periodic Table. Sb-based perovskites, commonly formulated as $A_3Sb_2X_9$ (where A represents MA^+ or Cs^+ and X represents I^-, Br^-, or Cl^-), have shown considerable promise for these applications. These materials exhibit favorable optoelectronic properties, positioning them as strong candidates for next-generation solar cell technologies.[190] Weber et al. reported the synthesis of interesting Sb-based perovskites $(Rb_3Sb_2Br_{9-x}I_x)$ for solar cells, exhibiting a monoclinic structure and $P2_1/n$ space group, which is consistent with the 2D crystal structure of $Rb_3Sb_2I_9$ (Fig. 9a). It was observed that with an increase in the bromide content in the BX_6 octahedron, the
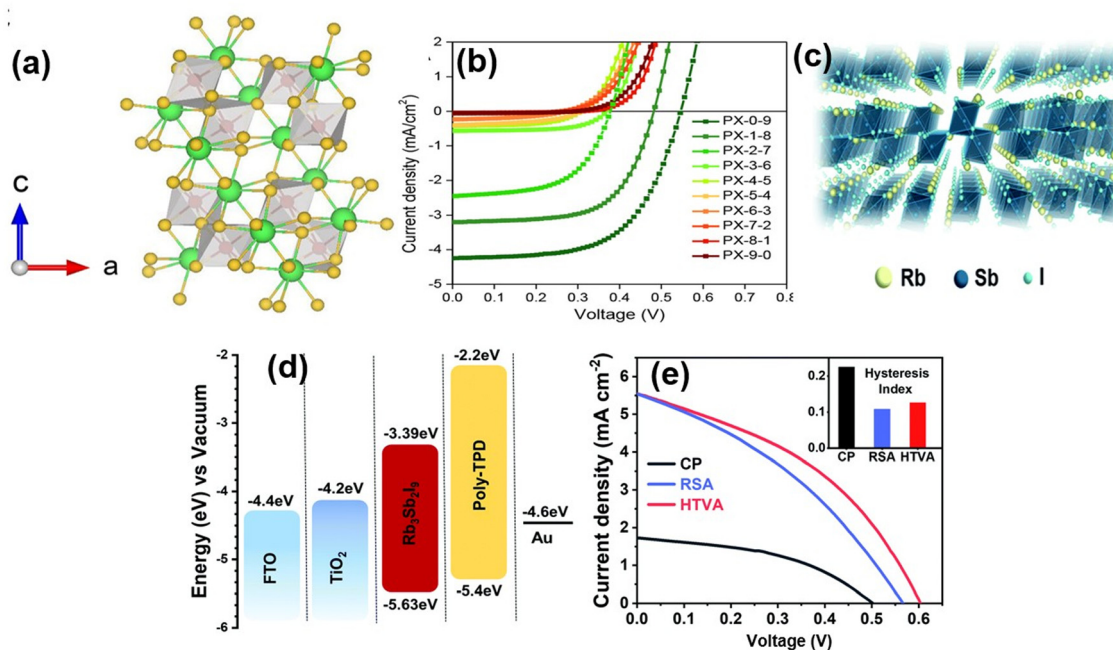
Fig. 9 (a) 2D crystal structure of $Rb_3Sb_2I_9$ (red, Sb; green, Rb; and yellow, I) and (b) $J–V$ curves of $Rb_3Sb_2Br_{9−x}I_x$-based solar cells. Reproduced with permission from ref. 170, copyright 2019, ACS. (c) Compact 2D structure of $Rb_3Sb_2I_9$, (d) energy band structure of $Rb_3Sb_2I_9$-based devices, and (e) $J–V$ characteristics of different $Rb_3Sb_2I_9$ devices. Reproduced with permission from ref. 162, copyright 2020, RSC.

perovskite volume readily decreased from $Rb_3Sb_2I_9$ to $Rb_3Sb_2Br_9$. The substitution of iodide with bromide started to shrink the unit cell with a blue shift in absorption profile and a larger band gap. It disoriented the crystallinity of the perovskites and formed a layered structure, which was detrimental to the charge mobility, leading to a decrease in the photovoltaic efficiency. Thus, the highest efficiency of 1.37% was achieved for the unmasked PX-0-9 perovskite solar cells (Fig. 9b).[170] Likewise, Li *et al.* reported the preparation of compact $Rb_3Sb_2I_9$ thin films with improved microstructure for lead-free perovskite devices through the deposition strategy, as presented in Fig. 9c. The high-quality thin film was developed by controlling the high-temperature annealing process and supersaturation level. The $Rb_3Sb_2I_9$ thin films attained a microstructural environment that increased the charge carrier mobility and reduce the charge recombination centers, thus boosting the photovoltaic performance. Thus, the PSC devices comprised of the $Rb_3Sb_2I_9$ thin-films achieved a significantly higher PCE value of 1.35% with a maximum EQE of 65.4% (Fig. 9d).[162] This indicated that thin film processing strategies can be effective in improving the microstructural and optoelectronic properties, subsequently enhancing the device performance. The resulting current density–voltage characteristics are presented in Fig. 9e.

Furthermore, our group developed a PSC device by fabricating MASbI perovskite as a light absorber.[171] The thin film was prepared by employing a two-step modified sequential deposition method. The MASbI-based PSC device exhibited a maximum efficiency of 0.54%, which is low compared to other reported Sb-based perovskites. However, the device exhibited an impressive V_{oc} of 740 mV, demonstrating the potential of

MASbI-based materials for future improvements in PSC performance.[171,172]

8. Double perovskites

To replace Pb-halide perovskites, another approach is the use of halide double perovskites. Double perovskites with the general formula of $A_2B'B''X_6$ were developed to address the complexity associated with lead substitution, where the A position is a large cation such as Cs^+, while the B' and B'' positions are either trivalent or monovalent cations, and the X component is a halide.[191] Due to their high stability and non-toxic nature, halide-based double perovskites have attracted significant attention for application in PSCs. Six adjacent octahedral derivatives of B^IX_6 or $B^{III}X_6$ units coordinate at intersections with different ions to develop a 3D perovskite structure. Examining various combinations of B' and B'' positions in $A_2B'B''X_6$ is anticipated to facilitate the development of efficient alternatives to lead-based halide perovskites.[192]

Since their initial synthesis in the 1970s, only a limited selection of double perovskites such as $Cs_2AgBiBr_6$ and Cs_2NaBiI_6 has been utilized in solar cell applications. When double perovskite materials are confined to single monolayers at the nanoscale, their stability and quantum size effects improve. This behavior is due to the elevated nanocrystal surface energy in their metastable phases. Firstly, Zhao *et al.* led a study to understand the optoelectronic properties of a series of double perovskites, Cs_2NaBX_6 (B = Sb, Bi; X = Cl, Br, I), by applying first-principles calculations, aiming to evaluate their potential for solar cell applications. Their studies predicted that these

perovskites exhibit large indirect band gaps, limiting their light absorption capabilities. However, the perovskite with iodide as the halide ion displayed a lower band gap than that with chloride and bromide halide. It was observed that bromide and iodide perovskites have positive formation enthalpies and can be stable under certain conditions. It was also revealed that the charge mobility of these perovskites is lower than that of lead-based perovskites and needs to be tuned to achieve high efficiency.[193] Later, G. Volonakis performed simulation studies of many double perovskites of the $Cs_2BiB''X_6$ and $CsSbB''X_6$ family, where X represents Cl, Br, and I.[194] Based on their results, $Cs_2BiAgCl_6$ was successfully synthesized, which consists of a face-centered cubic double perovskite. Theoretical calculations indicated that these double perovskites can serve as indirect bandgap semiconductors and possess tunable carrier effective masses in the visible absorption range, which was also confirmed through optical characterization of the synthesized $Cs_2BiAgCl_6$. An interesting comparison was executed by Yang *et al.* to prepare the $Cs_2AgBiBr_6$ double perovskite *via* solution-processing and vacuum sublimation for highly efficient lead-free PSCs. The solution-processed films demonstrated superior properties, including higher crystallinity, reduced bandgap, longer lifetimes, and enhanced charge carrier mobility, compared to the vacuum-sublimated films. Consequently, the optimized power conversion efficiency was 2.51% for the solution-processed films, which is comparatively higher than that of 1.41% for their vacuum-processed counterparts (Fig. 10a and b), respectively. This signified that the synthetic strategy can impact the precise composition stoichiometry and lead to a high-quality perovskite film, beneficial for photovoltaic performance.[180]

Since its discovery, $Cs_2AgBiBr_6$ has emerged as an important lead-free double perovskite material to address the stability and toxicity issues of lead halide perovskites. Ghasemi *et al.*
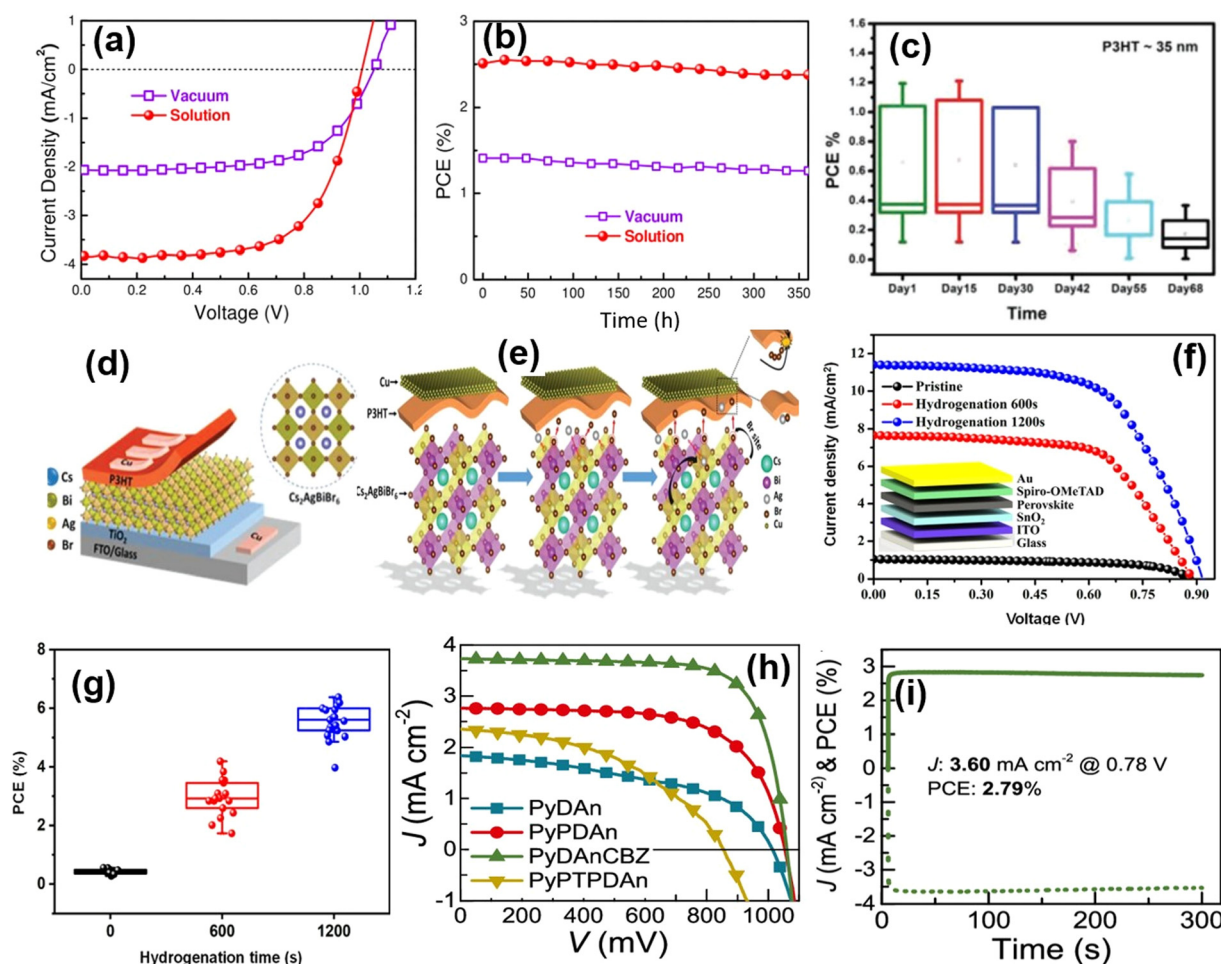

Fig. 10 (a) *J–V* curves of PSC devices fabricated and (b) ambient stability characteristics of the perovskite solar cells fabricated with optimized solution- and vacuum-processed $Cs_2AgBiBr_6$ thin films. Reproduced with permission from ref. 180, copyright 2019, ACS. (c) Statistics of device efficiency of 35 nm-thick P3HT films stored under atmosphere conditions, (d) device configuration of the $Cs_2AgBiBr_6$ solar cell, and (e) schematic of dual-ion-diffusion-induced degradation of $Cs_2AgBiBr_6$ in a PSC device. Reproduced with permission from ref. 181, copyright 2020, John Wiley and Sons. (f) *J–V* curve of $Cs_2AgBiBr_6$ PSCs with different hydrogenation times (0 s, 600 s and 1200 s). (g) Average photoelectric conversion efficiency (PCE) distribution of $Cs_2AgBiBr_6$ PSCs at different hydrogenation times, along with a layered PSC in the inset picture. Reproduced with permission from ref. 179, copyright 2022, Nature Commun. (h) *J–V* curves of $Cs_2AgBiBr_6$ solar cells with different HSLs. (i) Stabilized power output of PyDAnCBZ HSL. Reproduced with permission from ref. 177, copyright 2023, ACS.

developed a high-quality $Cs_2AgBiBr_6$ thin film for the fabrication of a lead-free double PSC, which exhibited an efficiency of 1.91% (Fig. 10c and d). However, the long-term stability of the PSC devices was affected by the dual-ion-diffusion-induced degradation of $Cs_2AgBiBr_6$, in which Ag and Br readily diffused through the HTL layer (Fig. 10e). Nevertheless, this phenomenon can be restricted by using a thick layer of hole-transporting material in the devices. This work emphasized the fundamental understanding of ion behavior to achieve high stability. Similarly, our group further explored $(CH_3NH_3)_3Sb_2I_9$ and $(NH_4)_3Sb_2I_9$ perovskites as light-absorbing materials to fabricate lead-free PSCs. Between them, the $(NH_4)_3Sb_2I_9$-based PSC devices demonstrated an improved PCE of 0.42% and a remarkable open-circuit voltage (V_{oc}) of 0.94 mV, highlighting the potential of $(NH_4)_3Sb_2I_9$ as an alternative for Pb-free PSCs.[181] The efficiency of $Cs_2AgBiBr_6$-based PSCs is normally lower because of its wide bandgap and limited light absorption area. Notably, Zhang et al. achieved a breakthrough in this regard and reported a stable hydrogenated $Cs_2AgBiBr_6$ lead-free double perovskite solar cell with a power conversion efficiency of 6.37% (Fig. 10f and g). $Cs_2AgBiBr_6$ films were successfully doped with atomic hydrogen via a hydrogenation method to lower the bandgap of the double perovskite from 2.18 to 1.64 eV. First-principles calculations suggested that H-atoms are integrated into the interstitial sites of the perovskite crystal and significantly enhance its optical properties, charge carrier mobility, and lifetime compared to the pristine perovskite structure. This demonstrated that an effective lattice engineering strategy for double perovskites can be beneficial to form highly stable and environment-friendly efficient PSCs with tunable optoelectronic properties.[179] Recently, Huang et al. fabricated modified $Cs_2AgBiBr_6$ PSC devices using different hole transporting layers. Four pyridine-based organic moieties with different functionalization at the 2,6-position of pyridine were investigated as the HTL for PSC application. Among them, PyDAnCBZ with carbazole functional moieties significantly improved the electro-optical properties and facilitated charge carrier transport in the PSC (Fig. 10h and i). Thus, the PyDAnCBZ-incorporated PSC device exhibited an improved power conversion efficiency of 4.9% with high thermal and moisture stability.[177]

Recently, Sekar et al. investigated the performance of a new $FA_4GeSbCl_{12}$ double perovskite solar cell using drift-diffusion SCAPS-1D simulation and achieved an efficiency of 22.5%. Their studies displayed that the device performance can be boosted by optimizing the band structure of the ETL and HTL layers and varying their thickness and defect density.[178] In a similar approach, Karmaker et al. introduced a novel $Cs_4CuSb_2Cl_{12}$ perovskite nanocrystal cell, a promising material for PSCs. Various numerical simulations were carried out to optimize the $Cs_4CuSb_2Cl_{12}$ nanocrystal-based solar cells, addressing the challenging task of balancing the device parameters. Their findings revealed that while thicker perovskite layers enhanced the light absorption, they also impeded the charge transport efficiency. Through computational modeling, this study optimized the key parameters, including perovskite layer thickness, doping material

concentration, and defect density. Further, the proposed PSC exhibited a PCE of 23.10% with a V_{oc} of 1.1675 V and fill factor (FF) of 83.33%.[73] Recently, Kong et al. reported a luminescence down-shifting lead-free $Cs_2Ag_xNa_{1-x}Bi_yIn_{1-y}Cl_6$ double perovskite phosphor (CANBIC) for silicon solar cells. The phosphor was incorporated into a polydimethylsiloxane (PDMS) film to improve the energy conversion in the ultraviolet (UV) spectrum. The CANBIC microcrystal served as a bifunctional fluorescent compound that absorbs light from the full solar spectrum through light scattering for silicon solar cells. By optimizing the CANBIC content in the textured PDMS film, an optical efficiency enhancement of 5.40% was obtained and the LSC-PV system showed a significant improvement in PCE, reaching up to 0.463% with a J_{sc} of up to 1.232 mA cm^{-2}. By using an Al foil, the LSC-4PV system further reached a champion efficiency of 3.14% with high photostability and air stability.[176]

9. Other lead-free perovskites

Despite the significant advancements in rare-earth-based lead-free perovskites, maintaining high luminescence stability remains a considerable challenge. Considering this challenge, Zhao and coworkers performed first principles calculations for Cs_2NaBX_6, where B represents Sb and Bi and X represents Cl, Br, and I to understand their electronic properties for the development of lead-free double perovskites. It was found that Cs_2NaSbI_6 and Cs_2NaBiI_6 perovskite have an indirect band gap of 1.65 and 1.68 eV, respectively, similar to the $Cs_2AgBiBr_6$ double perovskite. Furthermore, DFT calculations indicated that the mobility of holes in these double perovskite is lower than the corresponding photogenerated electrons, suggesting that their band structure and charge carrier mobility need to be optimized in terms of potential photovoltaic application.[193] In 2015, DFT studies were performed for AMX_3 using K, Rb, and Cs as the A cations and Cl, Br, and I as the halide anions to investigate their bandgap and stability. The calculations indicated that $RbSnBr_3$, $CsSnBr_3$, and $CsGeI_3$ are promising for solar cells. Among them, $CsGeI_3$ possesses the optimal bandgap but displays a low PCE value. Many alkaline metals such as Ca, Sr, and Ba can be interesting elements for the synthesis of lead-free perovskite materials. They are usually low-cost and beneficial for large-scale applications. The Sr^{2+} and Ca^{2+} cations have the capability to form perovskites and are more stable compared to Sn and Ge. T. Edvinsson et al. investigated the simulation calculation of the structural and optoelectronic properties of $CH_3NH_3SrI_3$ and $CH_3NH_3PbI_3$. The DFT analysis revealed that the bandgap of $CH_3NH_3SrI_3$ is large given that Sr^{2+} is less electronegative and has an empty d-orbital. Moreover, the formation of Sr-based perovskites was unsuccessful given that metal iodine bonding restricts the interaction of MA with strontium.[195]

Transition metals were predominantly investigated for Pb replacement in lead-free perovskite due to their tendency to form complex through vacant d-orbitals. Cui et al. applied a low-temperature solution-based technique to synthesize

copper-based perovskites, $(p\text{-F-C}_6\text{H}_5–\text{C}_2\text{H}_4\text{NH}_3)_2\text{CuBr}_4$ and $(\text{CH}_3(\text{CH}_2)_3\text{NH}_3)_2\text{CuBr}_4$, which possessed an optimal band gap of 1.75 for photovoltaic application. However, the PSC devices fabricated using these perovskites exhibited low PCE values of 0.51% and 0.63%, respectively.[196] Later, N. Mathew reported the synthesis of a series of copper-based layered 2D perovskites, $(\text{CH}_3\text{NH}_3)_2\text{CuCl}_x\text{Br}_{4−x}$, using different ratios of halide ions for bandgap optimization and tuning their optoelectronic properties. These perovskites were easily deposited as highly oriented films *via* the spin coating method. Cu^{2+} was converted to Cu^+ during the annealing process due to the presence of the bromide ion, which increased the green photoluminescence properties. Among them, $(\text{CH}_3\text{NH}_3)_2\text{CuCl}_2\text{Br}_2$-based PSC device exhibited a power conversion efficiency of 0.017%.[197] Our group also reported the synthesis of organic–inorganic copper(II)-based perovskites, $\text{C}_6\text{H}_4\text{NH}_2\text{CuBr}_2\text{I}$ and $\text{C}_6\text{H}_4\text{NH}_2\text{CuCuCl}_2$, for the fabrication of perovskite solar cells. Both perovskites showed absorption in the region of 400–700 nm with band gaps of 1.65 eV and 2.01 eV, respectively. These perovskites were utilized as light absorbers in PSC devices with ZnO as the HTL layer, exhibiting a PCE value of 0.42% and 0.61%, respectively, which was comparatively higher than that of TiO_2-based devices.[198] Further, Wilett *et al.* studied the magnetic properties of two iron-based 2D perovskites but their material application remained unexplored.[199] Mn-based perovskites can also be good photovoltaics considering their absorption region in the visible and UV regions. Considering this, Zhou *et al.* prepared a $\text{CH}_3\text{NH}_3\text{MnI}_3$ (a-MAMnI_3) thin film *via* the spin coating technique and developed a photovoltaic device. This device showed a PCE of 0.02% and V_{oc} of 0.33 V, indicating that Mn-based perovskites may have potential for application in solar cells.[200] The Zhigang Zang group propose an alternative saturated precursor cyclic crystallization method to prepare centimeter-sized CsCu_2I_3 single crystals (SCs) with a one-dimensional (1D) structure. Their report revealed unidirectional and efficient charge carrier transport in the 1D CsCu_2I_3 SCs, and consequently the CsCu_2I_3 SC-based detector exhibited an excellent X-ray detection performance.[12]

Palladium and titanium are also viable options for the fabrication of lead-free PSCs. Ju and coworkers synthesized several Ti^{4+}-based perovskites, $\text{Cs}_2\text{TiI}_x\text{Br}_{6−x}$ ($x = 0, 2, 4, 6$) *via* a melt-crystallization method and studied their potential for photovoltaic application. Among them, the $\text{Cs}_2\text{TiI}_2\text{Br}_4$ perovskite attained a bandgap of 1.38 eV, making it suitable for use in single-junction solar cells. Ti-based perovskites displayed excellent light absorption capability, absorption behavior, defect density, and high carrier mobilities comparable to lead-based perovskites and can serve as light absorber layers in PSC devices considering their carrier mobilities.[201] Furthermore, Huang *et al.* synthesized the $(\text{CH}_3\text{NH}_3)_2\text{PdCl}_3$ perovskite *via* a low-temperature solution method. It formed a 2D layered phase with a high absorption coefficient and was stable in air, making it advantageous to several existing perovskites. However, it possessed a direct bandgap of $\sim$2.2 eV, limiting its potential for solar applications but this can be tuned by replacing its halide ion.

Recent studies have shown that the performance of PVSCs is highly related to the existence of Pb^{2+} ions. Simply substituting lead with other metal cations typically results in a significant deterioration in device efficiency. However, mixed Pb–Sn perovskites can maintain relatively high efficiency. Mixed metal cations and halide double perovskites featuring a 3D structure should exhibit a good charge transport performance, although more research is needed. Overall, although many challenges have been identified, many more remain unaddressed, and thus the further development of lead-free materials with comparable performances to Pb-based perovskites is required.

10. Defect ordered perovskites

The defect properties in lead-free perovskite materials have been actively investigated because their unavoidable presence in the active layer highly impacts the performance of PSCs. A change in the 0D configuration to 2D layered structure in $\text{A}_3\text{B}_2\text{X}_9$ defected perovskites, along with enhanced electronic dimensionality, markedly improves the performance of the corresponding PSCs.[202] In PSCs, deep-level defects primarily serve as recombination centers, reducing the carrier lifetime and limiting the device performance. In contrast, shallow-level defects function as donors or acceptors and contribute to the generation and transportation of charge carriers. Bismuth exhibits defects due to its oxidation state and presence of lone pairs and has possibly benign properties, demonstrating less toxicity, and thus making it as effective as a heavy metal. Excessive exposure to MAI vapor led to a reduction in Bi-based metal defect sites, thereby decreasing the recombination losses. Defects in $\text{Cs}_3\text{Bi}_2\text{I}_9$ exhibit low formation energies and a propensity to introduce deep-level states within the bandgap, leading to significant carrier recombination. Scanning tunneling spectroscopy revealed that the band edges of the $\text{Cs}_3\text{Bi}_2\text{I}_9$ perovskite exhibit p-type characteristics, which is attributed to the electron-accepting nature of the defects located above the valence band. However, when methylammonium (MA) occupies the A positions, defect formation becomes less favorable because of the defect-tolerant properties of MA-based perovskites.[203] As a result, the defect-related challenges are effectively mitigated by transitioning $\text{A}_3\text{B}_2\text{X}_9$ from a zero-dimensional dimer configuration to a 2D structure. Furthermore, the improved phase purity of the 2D layered configuration contributes to a decrease in defect density.[204]

In addition to point defects, interfacial defects play a critical role in device performance, predominantly occurring at the grain boundaries where their density is significantly higher than within the grains. As the grain size increases and the number of grain boundaries decreases, perovskite films contain a lower defect density, thereby minimizing the recombination rate and improving the PCE. To reduce the deep-energy-related defects or interfacial defects, several methods have been employed, thus enhancing the optoelectronic properties. Materials engineering, *i.e.*, structural engineering by varying the cations (MA, FA, and Cs) and anions (Cl, Br, I) in perovskites,
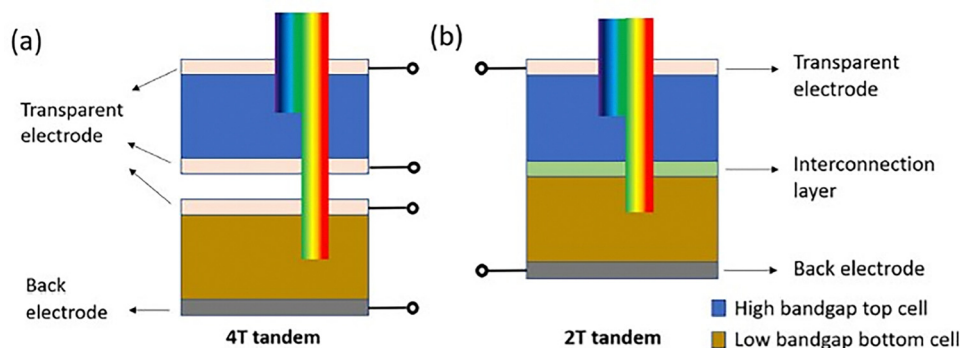
Fig. 11 Schematic of two types of two-junction tandem configurations: (a) four-terminal (4T) mechanically stacked tandem and (b) two-terminal (2T) monolithically integrated tandem. Reproduced with permission from ref. 207, copyright 2021, AIP.

has been proven to be an effective approach for enhancing the performance and stability of PSCs. High-efficient solar cells incorporating these mixed perovskites demonstrate a reduction in defects and enhanced defect tolerance.[205,206]

11. Tandem solar cells

Additionally, multi-junction devices, such as tandem solar cells, are widely regarded as a promising approach to achieve higher power conversion efficiencies and surpass the Shockley–Queisser efficiency limit inherent to single-junction devices.[207] In tandem solar cell configurations, high-energy and low-energy photons can be efficiently captured by the front and rear subcells, respectively, which are designed with complementary bandgaps. Subsequently, these photons are converted into electrical energy and collected through a transparent interconnecting layer or internal electrode, enabling enhanced photon utilization and improved overall device performance.[208] For constructing tandem devices by themselves or interfacing with a variety of solar cells, tunable bandgaps in the range of 1.17 to 2.3 eV are required. The bandgap can also be tuned *via* compositional engineering, which make perovskites highly desirable for tandem cell applications. Some reports on copper indium gallium selenide (CIGS) perovskites,[209,210] Si-based perovskites,[211,212] and perovskite–organic-photovoltaic (OPV) tandems[213,214] have demonstrated promising energy conversion efficiencies. Two different types of configurations are used to fabricate these perovskite-containing tandem solar cells, *i.e.* monolithic 2-terminal tandems, which electrically connect two subcells through a transparent internal electrode, and mechanically stacked 4-terminal tandems, where the two cells are fabricated independently, and then mechanically stacked on top of each other. The incorporation of an additional transparent electrode in four-terminal devices introduces increases the optical absorption losses and elevates the overall fabrication costs, posing challenges for their practical implementation and scalability.[215] In contrast, the challenges inherent to two-terminal perovskite tandem solar cells encompass the design and integration of an efficient charge recombination interlayer, the intricate fabrication process involving multiple layers, and the precise optimization of the optical and electrical

properties of the thick subcells to achieve the optimal performance. Multi-junction tandem solar cells utilize a stacked configuration of photovoltaic subcells with varying bandgap energies, enabling each subcell to selectively absorb distinct spectral regions of sunlight. This design optimizes the photon utilization by minimizing the sub-bandgap transmission losses and reducing thermalization losses, thereby enhancing the overall energy conversion efficiency.[207] Fig. 11a and b illustrate two configurations for double-junction tandem cells. A double-junction tandem solar cell represents the most fundamental configuration within the multi-junction architecture, which can be fabricated by mechanically stacking the high-bandgap cell on top of the low-bandgap cell. A monolithically integrated tandem solar cell represents a more sophisticated and streamlined approach, which is typically achieved by directly fabricating a high-bandgap subcell on a low-bandgap subcell. This integration facilitates efficient charge carrier transport and minimizes the optical losses, thereby enhancing the overall performance and scalability of the tandem architecture.[216] Hybrid metal halide perovskite solar cells have recently emerged as highly promising candidates for multi-junction tandem applications, driven by their rapid advancements in power conversion efficiency (PCE), which has reached 26%.[215] To enhance the performance of perovskite solar cells (PSCs), the development of tandem solar cell architectures represents a promising strategy for augmenting the power conversion efficiency (PCE) of existing photovoltaic technologies, while maintaining cost-effectiveness.[217,218]

12. Challenges and strategies

Lead-free halide perovskites have emerged as ideal options to replace lead-based perovskites and have developed tremendously in the last decade. However, despite the recent advances in lead-free perovskites, they still lag behind lead-based perovskites in terms of efficiency and stability. There are many challenges in lead-free perovskite regarding their synthetic strategies, poor morphology, weak optoelectronic properties, stability under environmental conditions, cost-effectiveness, and scalability for practical application. The following points explain the pressing challenges in the field of lead-free

perovskite solar cells, and also provide strategies to tackle them from distinct perspectives.

12.1. Stability issue

Despite attaining high PCEs, the stability of lead-free perovskites under atmospheric conditions poses a major issue, preventing the large-scale application of PSCs and their commercialization. Sn^{2+} and Ge^{2+} in perovskite solar cells easily oxidize into Sn^{4+} and Ge^{4+}, respectively, in the presence of air and under degradation at room temperature, making the PSC devices highly unstable.[219,220] Lead-free PSCs must be operational for longer times, such as days or years, to replace the traditional solar cells. Thus, to counter this problem, doping or alloying of Sn-based perovskites can be performed to effectively suppress the oxidation process.[221] Further, utilizing organic ligands or self-assembled monolayers can also reduce defect formation and suppress oxidation to stabilized these materials.[222] In the case of doping or incorporation of additives, bipyridine-based organic/inorganic complexes can play an important role in perovskites because bipyridine can coordinate with Sn^{2+} and inhibit its conversion to Sn4+, enhancing the stability of Sn-based perovskites.[223] Additionally, it also serves to optimize the band gap, lower the binding energy, and enhance the transportation and lifetime of charge carriers, resulting in high photovoltaic performances. Additives such as SnF_2 were mostly added in low amounts for stabilizing tin-based perovskites. Incorporating excessive halides during the fabrication process can mitigate the performance issue because they suppress the oxidation, and thereby enhance the stability of the perovskite structure, improving the overall device performance. Some studies have shown that the addition of halides, particularly "fluoride", significantly reduced the rate of degradation under conditions of high humidity and elevated temperatures.[224] Using excess of halide ions such as Cl^-/Br^- in the perovskite precursor can also produce the same effect. Further, halides can also improve the morphology, passivate defects, and influence the crystallization process, leading to better charge transport properties and enhancing the structural integrity to increase the efficiency.[225] Further, Bi and Sb-based perovskites do not undergo degradation *via* the oxidation process and exhibit great stability in air and moisture, and thus PSC devices with Bi and Sb perovskites need to be further explored. Also, Sb is considered an auspicious substitute for lead-based perovskites with enhanced performances[226] but there are still challenges that need to be addressed to produce efficient perovskite solar cells. For example, Sb devices are solution-processed, favouring the dimer phase, which exhibits poor photovoltaic properties.[227] It has also been found that inorganic cations possess better stability compared to organic cations, especially high thermally stable. Therefore, more perovskite cells with cesium or Rb cations rather than organic cations need to be developed for PSC application. Likewise, inorganic halide perovskites show excellent stability compared to organic–inorganic hybrid halide perovskites.

12.2. Synthetic strategy modification

To achieve a high power conversion efficiency (PCE), the formation of high-quality thin films with high crystallinity and minimum defect density is a necessary but challenging target.

The synthetic methodology plays a vital role in producing high-quality perovskite thin films with zero defects, uniform morphology, and high stability.[228,229] Simple or inexpensive methods such as the solvothermal and hydrothermal methods are not beneficial for developing lead-free perovskite solar cells. Solution processing, spin coating, and vapour deposition are widely known techniques for the fabrication of high-quality perovskite thin films. For example, Ran *et al.* developed a two-step evaporation-spin-coating film fabrication technique, where they observed a low FF, which is still a challenge. This might be because of the high trap-state density, short carrier diffusion length, and low charge mobility in the thin film.[230] However, Sn-based thin films undergo faster crystallization during their synthesis, which often results in low stability and poor photovoltaic performances. The vapour deposition method forms a uniform morphology of perovskite thin films with different scale lengths and minimum pinhole generation, subsequently obtaining better photovoltaic performances.[231] Interestingly, one of the effective strategies is to combine the solution and vapor-deposition methods, which enables slow film growth to acquire high-quality thin films. Besides, significant efforts have been dedicated to forming thin films free of pinholes with the minimum defect density, while controlling their grain size and structure dimensionality, which results in high performances in lead-free perovskite-based PSC devices. Furthermore, it was discussed in the previous section that the incorporation of additives, doping or alloying was implicated in the production of smooth and crystalline thin films with a large coverage area, optimal band structure, high charge mobility and improved stability under ambient conditions, developing high-efficient PSC devices. Owing to these developed fabrication methods, there has been significant advancement in lead-free perovskite solar cells in terms of quality and device with a small area, but scalability remains the main issue for their large-scale application. For progress towards real applications, continuous efforts are necessary to develop crystalline lead-free perovskite films in large areas with good reproducibility.

12.3. Improvement in optical properties

Fabrication strategies for perovskite materials should yield high-quality films with excellent optoelectronic properties by controlled nucleation and crystal growth. One of the major challenges is to tune the optoelectronic properties of perovskite materials in terms of their absorption coefficient, band structure, charge mobility, carrier lifetimes, *etc*.[232,233] In the aspects of absorption coefficient and band gap tuning, different strategies have been employed, such as modulation of the cation and anion sites and high-quality thin film formation. Addition of reducing or additives with perovskite material might be very effective to increase absorption in the solar spectrum. (example needed) Regarding the charge mobility and carrier lifetimes, perovskites exhibit a high excitation binding energy, which restricts the free movement of photogenerated electrons and holes and retards the charge mobility. This limits the photovoltaic performance of lead-free halide perovskites compared to lead-based perovskites. High-quality thin films with crystalline

growth and uniform grain size possess greatly a minimized defect density, which significantly reduces the recombination of excitons and exciton carrier lifetimes and increases the charge mobility, thus enhancing the device performance. Alternatively, the choice of appropriate hole transporting materials (HTMs), surface passivation, and additive engineering are also important to realize efficient charge transportation. Notably, the incorporation of photosensitizers and dye in perovskite solar cells can be effective to tune their optical properties, which can lead to broader absorption in the UV-visible region, efficient charge migration, longer lifetimes and stability in PSC devices, drastically improving the cell performance.

12.4. Theoretical aspect

The formation of perovskite materials is dependent on trial-based methods, and sometimes, expected results are not produced from newly developed PSC devices. In this direction, theoretical calculations and new methodologies such as DFT studies, artificial intelligence, and machine learning can be helpful to assist in designing perovskite materials with desirable properties. A data-driven screening of possible perovskites from simulation studies based on a preliminary perovskite design or literature reports might open new avenues and encourage the development of highly efficient perovskite solar cells. Also, it might be helpful to gain information about structural and electronic properties, such as how organic and inorganic cations impact the optical or electronic properties of perovskites. Ge-based inorganic perovskites, $AGeX_3$ (A = Cs or Rb; X = I, Br, or Cl), were investigated by theoretical simulation to calculate their absorption coefficients, exciton binding energies, and band gaps, which predicted their behaviour as light absorber materials. Recently, theoretical investigations have attracted significant attention in synthetic chemistry, which holds promise to revolutionize this field.

12.5. Scalability

There is growing interest in the synthesis of perovskites for solar cells, but most synthetic strategies cannot facilitate large-scale production and are only limited to the milligram level, thereby restricting their scalability and practical applications. One of the serious issues with PSCs are large-area processing and scaling-up, which restrict their practical applications. Thus, to mitigate these challenges, potential strategies need to be employed such as doping, which stabilizes the perovskite lattice and reduces oxidation, and use of reducing agents that may prevent oxidation in lead-free PSCs.[234] Spin-coating is a popular method for synthesizing lead-free halide perovskite solar cells, but it is not suitable at the large-scale level due to its high tangential velocity. In the context of large-area processing and scaled-up deposition, techniques such as blade coating are employed to fabricate large-area devices, which can help stabilize flexible perovskite solar modules. Growth control and composition and inferential engineering can improve the large-area processing of lead-free PSCs.[235] To overcome the issue of scaling-up, work on surface passivation techniques, reducing agents, and chemical modifications can help to enhance the stability and efficiency.[236]

Modifying the device architecture and incorporating additives into the perovskite precursor solution can help scale-up the process.[237] Synthetic methodologies such as spray coating, slot-die coating, inkjet printing, and soft film coating have also been employed for the realization of large-scale perovskite film development. These strategies for fabricating perovskite films are cost-effective, efficient, and straightforward and mostly explored for lead-based perovskites. However, significant progress has been made for lead-free perovskites with better device performances, but the above-mentioned methods also need to be explored.

To summarize these challenges and strategies, lead-free PSCs exhibit lower PCEs compared to lead-based halide perovskites because they possesses an indirect band gap, very low carrier mobility and short charge carrier diffusion length, which further affect the device performance. Thus, many other strategies have been applied to overcome these barriers including the use of a reducing agent, introduction of additives, solvent and device structure engineering, and use of 2D structural components.[237,238] Numerous fabrication techniques can help boost the PCEs. Sn-based perovskites have now achieved an efficiency of more than 15%, while other lead-free Bi, Sb, and Ge-based perovskites is approaching 5% due to the modifications of (a) the addition of an anti-solvent, which accelerates heterogeneous supersaturation, nucleation, and precipitation processes, leading to a more uniform, pinhole-free crystal morphology with enhanced PCE, (b) uniform morphology of compact films and well-defined grain boundaries and (c) modification of A–and X-site mixing.

13. Summary and future outlook

Owing to the toxic nature of lead-based perovskites for PSCs, this feature article attempted to provide a concise overview of the applications of lead-free PSCs to significantly expand the panorama of possible metals such as Sn, Bi, Sb, and Ge, among which Sn is the major player to achieve a sustainable future for PSCs. These lead-free PSC materials are attracting increasing attention because of their nontoxicity and outstanding performances. Some significant parameters for the champion device require a low background density charge carrier, appropriate band gap, high absorption coefficient, effective carrier transport, and stronger stability in the ambient atmosphere. This review presented bright insight into the advantages and limitations of Pb-free perovskites, the present status, impact of the cations at the A, B, and X sites, up-to-date progress, challenges, strategies, and outlook in lead-free perovskite materials for solar cell applications. In 2009, the birth of PSCs certainly prefigured a new edge for next-generation photovoltaics. In the past one and half decades, the PCE of PSCs increased from the initial 3.8% to 26% with a great change from 2-dimensional to 3-dimensional structures along with liquid to solid junctions. Lead-free PSCs are a promising candidates because of their more stable phase and highly attractive based on existing technology. Large-area processing and scale-up technology has become a tricky problem that needs to be addressed before commercialization. To date, researchers have been focused on

devices having large areas and uniform films because their efficiency is still poor. However, many of the film-making techniques including drop-casting and spin-coating used in different laboratories do not suit large-scale production. The printing and spraying techniques are considered promising methods for scale-up but scaling up the size of PSCs without the significant loss of efficiency is a challenge needs to be resolved. All perovskites must be environment-friendly and not harm the human body like Pb. Enhancing the stability of manufacturing long-lasting PSC devices with a high PCE is still an urgent issue to be implemented. To advance the development of integrated photovoltaics, numerous studies have focused on all-perovskite solar cells; however, research on inorganic PSCs remains relatively limited. Excellent PCEs have been achieved thus far for lead-free perovskites. However, they exhibit poor stability, and thus researchers are devoting great efforts to overcome this problem, such as using reducing agents to inhibit oxidation and excess amounts of halide to produce a rich environment. To improve the film quality of tin-based PSCs, additives can be introduced, significantly enhancing the device performance. At the beginning of this review, we discussed the synthesis of lead-free perovskite solar cells and their essential optical characteristics, together with the impact of the A-site cations on their chemical modification, which can not only improve the perovskite film morphology and device performance but also increase its long-term stability. Epitaxial growth-like techniques can play a pivotal role in improving the perovskite crystallinity, which is effective in improving the device performance. A few challenges exist and researchers have devoted great efforts to settle them to date. Moreover, to improve the performance of lead-free-based PSCs, we need to consider more effective approaches to overcome their limitations. In the last few years, the J_{sc}, FF (fill factor), PCE, V_{oc} and device stability of solar cells have been enhanced by utilizing different approaches. Interfacial defects play a crucial role in improving the power conversion efficiency (PCE) of these devices. For commercialization, all the discussed lead-free perovskite materials seem to be promising alternatives because of their less toxicity, good stability, and reasonable optoelectronic properties. Preparing these types of lead-free perovskites will be a significant step toward developing high-efficiency lead-free perovskite cells.

Data availability

The original data are available upon request and can be obtained by contacting the corresponding author.

Conflicts of interest

There are no conflicts to declare.

Acknowledgements

References

1 N. Kannan and D. Vakeesan, *Renewable Sustainable Energy Rev.*, 2016, **62**, 1092–1105.
2 A. Striolo and S. Huang, *J. Phys. Chem. C*, 2022, **126**, 21527–21541.
3 M. A. Green, *Nat. Energy*, 2016, **1**, 1–4.
4 C. Ballif, F.-J. Haug, M. Boccard, P. J. Verlinden and G. Hahn, *Nat. Rev. Mater.*, 2022, **7**, 597–616.
5 C. Isabela, R. A. M. Lameirinhas, J. P. N. Torres and C. A. Fernandes, *Sustainable Energy Fuels*, 2021, **5**, 2273–2283.
6 N. Papež, R. Dallaev, Ş. Ţălu and J. Kaštyl, *Mater*, 2021, **14**, 3075.
7 A. B. Muñoz-García, I. Benesperi, G. Boschloo, J. J. Concepcion, J. H. Delcamp, E. A. Gibson, G. J. Meyer, M. Pavone, H. Pettersson and A. Hagfeldt, *Chem. Soc. Rev.*, 2021, **50**, 12450–12550.
8 K. Yoshikawa, H. Kawasaki, W. Yoshida, T. Irie, K. Konishi, K. Nakano, T. Uto, D. Adachi, M. Kanematsu and H. Uzu, *Nat. Energy*, 2017, **2**, 1–8.
9 L. X. Chen, *ACS Energy Lett.*, 2019, **4**, 2537–2539.
10 J. Y. Kim, J.-W. Lee, H. S. Jung, H. Shin and N.-G. Park, *Chem. Rev.*, 2020, **120**, 7867–7918.
11 K. Galkowski, A. Surrente, M. Baranowski, B. Zhao, Z. Yang, A. Sadhanala, S. Mackowski, S. D. Stranks and P. Plochocka, *ACS Energy Lett.*, 2019, **4**, 615–621.
12 B. Wang, X. Yang, R. Li, S. M. Qaid, W. Cai, H. Xiao and Z. Zang, *ACS Energy Lett.*, 2023, **8**, 4406–4413.
13 T.-B. Song, T. Yokoyama, C. C. Stoumpos, J. Logsdon, D. H. Cao, M. R. Wasielewski, S. Aramaki and M. G. Kanatzidis, *J. Am. Chem. Soc.*, 2017, **139**, 836–842.
14 Y. Yang, H. Dai, F. Yang, Y. Zhang, D. Luo, X. Zhang, K. Wang, X. W. Sun and J. Yao, *Nanoscal. Res. Lett.*, 2019, **14**, 1–8.
15 W. Zhang, Y. Sui, B. Kou, Y. Peng, Z. Wu and J. Luo, *ACS Appl. Mater. Interfaces*, 2019, **12**, 9141–9149.
16 L. Zhou, J. F. Liao, Z. G. Huang, J. H. Wei, X. D. Wang, W. G. Li, H. Y. Chen, D. B. Kuang and C. Y. Su, *Angew. Chem.*, 2019, **131**, 5331–5335.
17 S. Zhao, W. Cai, H. Wang, Z. Zang and J. Chen, *Small Methods*, 2021, **5**, 2001308.
18 Y. Zhou, J. Chen, O. M. Bakr and O. F. Mohammed, *ACS Energy Lett.*, 2021, **6**, 739–768.
19 J. Petrulevicius, Y. Yang, C. Liu, M. Steponaitis, E. Kamarauskas, M. Daskeviciene, A. S. Bati, T. Malinauskas, V. Jankauskas and K. Rakstys, *ACS Appl. Mater. Interfaces*, 2024, **16**, 7310–7316.
20 J. Xu, H. Chen, L. Grater, C. Liu, Y. Yang, S. Teale, A. Maxwell, S. Mahesh, H. Wan and Y. Chang, *Nat. Mater.*, 2023, **22**, 1507–1514.
21 W. Ke and M. G. Kanatzidis, *Nat. Commun.*, 2019, **10**, 965.
22 S. Zhao, Z. Jia, Y. Huang, Q. Qian, Q. Lin and Z. Zang, *Adv. Funct. Mater.*, 2023, **33**, 2305858.
23 B. Saparov and D. B. Mitzi, *Chem. Rev.*, 2016, **116**, 4558–4596.
24 S. Ahmed, M. Gondal, A. Alzahrani, M. Parvaz, A. Ahmed and S. Hussain, *ACS Appl. Energy Mater.*, 2024, **7**, 1382–1397.
25 A. Kojima, K. Teshima, Y. Shirai and T. Miyasaka, *J. Am. Chem. Soc.*, 2009, **131**, 6050–6051.
26 M. M. Lee, J. Teuscher, T. Miyasaka, T. N. Murakami and H. J. Snaith, *Science*, 2012, **338**, 643–647.
27 Q. Jiang, J. Tong, Y. Xian, R. A. Kerner, S. P. Dunfield, C. Xiao, R. A. Scheidt, D. Kuciauskas, X. Wang and M. P. Hautzinger, *Nature*, 2022, **611**, 278–283.
28 Z. Xu, Z. Guo, H. Li, Y. Zhou, Z. Liu, K. Wang, Z. Li, H. Wang, S. M. Qaid and O. F. Mohammed, *Energy Environ. Sci.*, 2025, **18**, 1354–1365.
29 H. Yang, Z. Xu, H. Wang, S. M. Qaid, O. F. Mohammed and Z. Zang, *Adv. Mater.*, 2024, **36**, 2411721.
30 M. Green, E. Dunlop, J. Hohl-Ebinger, M. Yoshita, N. Kopidakis and X. Hao, *Prog. Photovoltaics*, 2021, **29**, 3–15.

31 C. Deline, D. Jordan, B. Sekulic, J. Parker, B. McDanold and A. Anderberg, *PV Lifetime Project-2024 NREL Annual Rep*, National Renewable Energy Laboratory (NREL), Golden, CO (United States), 2024.

32 Y. Li, L. Ji, R. Liu, C. Zhang, C. H. Mak, X. Zou, H.-H. Shen, S.-Y. Leu and H.-Y. Hsu, *J. Mater. Chem. A*, 2018, **6**, 12842–12875.

33 S. Yang, W. Fu, Z. Zhang, H. Chen and C.-Z. Li, *J. Mater. Chem. A*, 2017, **5**, 11462–11482.

34 M. M. Byranvand, C. Otero-Martínez, J. Ye, W. Zuo, L. Manna, M. Saliba, R. L. Hoye and L. Polavarapu, *Adv. Opt. Mater.*, 2022, **10**, 2200423.

35 L. Mao, C. C. Stoumpos and M. G. Kanatzidis, *J. Am. Chem. Soc.*, 2018, **141**, 1171–1190.

36 J. Li, H.-L. Cao, W.-B. Jiao, Q. Wang, M. Wei, I. Cantone, J. Lü and A. Abate, *Nat. Commun.*, 2020, **11**, 310.

37 F. Giustino and H. J. Snaith, *ACS Energy Lett.*, 2016, **1**, 1233–1240.

38 A. E. Magdalin, P. D. Nixon, E. Jayaseelan, M. Sivakumar, S. K. N. Devi, M. Subathra, N. M. Kumar and N. Ananthi, *Results Eng.*, 2023, 101438.

39 C. Zhang, L. Gao, S. Hayase and T. Ma, *Chem. Lett.*, 2017, **46**, 1276–1284.

40 R. Nie, R. R. Sumukam, S. H. Reddy, M. Banavoth and S. I. Seok, *Energy Environ. Sci.*, 2020, **13**, 2363–2385.

41 C. H. Chen, S. N. Cheng, L. Cheng, Z. K. Wang and L. S. Liao, *Adv. Energy Mater.*, 2023, **13**, 2204144.

42 M. M. Byranvand, W. Zuo, R. Imani, M. Pazoki and M. Saliba, *Chem. Sci.*, 2022, **13**, 6766–6781.

43 M. Wang, W. Wang, B. Ma, W. Shen, L. Liu, K. Cao, S. Chen and W. Huang, *Nano-Micro Lett.*, 2021, **13**, 1–36.

44 X. Jiang, Z. Zang, Y. Zhou, H. Li, Q. Wei and Z. Ning, *Acc. Mater. Res.*, 2021, **2**, 210–219.

45 M. S. A. Azizman, A. W. Azhari, D. S. C. Halin, N. Ibrahim, S. Sepeai, N. A. Ludin, M. N. M. Nor and L. N. Ho, *Synth. Met.*, 2023, **299**, 117475.

46 P.-K. Kung, M.-H. Li, P.-Y. Lin, J.-Y. Jhang, M. Pantaler, D. C. Lupascu, G. Grancini and P. Chen, *Sol. RRL*, 2020, **4**, 1900306.

47 X. Yang, W. Wang, R. Ran, W. Zhou and Z. Shao, *Energy Fuels*, 2020, **34**, 10513–10528.

48 L. Chouhan, S. Ghimire, C. Subrahmanyam, T. Miyasaka and V. Biju, *Chem. Soc. Rev.*, 2020, **49**, 2869–2885.

49 D. Kumar, R. S. Yadav, A. K. Singh and S. B. Rai, *Perovskite Mater., Devices Integr.*, 2020, (4), 190.

50 G. Nasti and A. Abate, *Adv. Energy Mater.*, 2020, **10**, 1902467.

51 S. Hu, K. Otsuka, R. Murdey, T. Nakamura, M. A. Truong, T. Yamada, T. Handa, K. Matsuda, K. Nakano and A. Sato, *Energy Environ. Sci.*, 2022, **15**, 2096–2107.

52 Z. Chen, J. J. Wang, Y. Ren, C. Yu and K. Shum, *Appl. Phys. Lett.*, 2012, **101**, 093901.

53 N. K. Noel, S. D. Stranks, A. Abate, C. Wehrenfennig, S. Guarnera, A.-A. Haghighirad, A. Sadhanala, G. E. Eperon, S. K. Pathak and M. B. Johnston, *Energy Environ. Sci.*, 2014, **7**, 3061–3068.

54 P. Wang, F. Li, K. J. Jiang, Y. Zhang, H. Fan, Y. Zhang, Y. Miao, J. H. Huang, C. Gao and X. Zhou, *Adv. Sci.*, 2020, **7**, 1903047.

55 W. Zhang, Y. Cai, H. Liu, Y. Xia, J. Cui, Y. Shi, R. Chen, T. Shi and H. L. Wang, *Adv. Energy Mater.*, 2022, **12**, 2202491.

56 Z. Kang, Y. Tong, K. Wang, Y. Chen, P. Yan, G. Pan, P. Müller-Buschbaum, L. Zhang, Y. Yang and J. Wu, *ACS Mater. Lett.*, 2023, **6**, 1–9.

57 B. B. Yu, Z. Chen, Y. Zhu, Y. Wang, B. Han, G. Chen, X. Zhang, Z. Du and Z. He, *Adv. Mater.*, 2021, **33**, 2102055.

58 T. Krishnamoorthy, H. Ding, C. Yan, W. L. Leong, T. Baikie, Z. Zhang, M. Sherburne, S. Li, M. Asta and N. Mathews, *J. Mater. Chem. A*, 2015, **3**, 23829–23832.

59 W. Ming, H. Shi and M.-H. Du, *J. Mater. Chem. A*, 2016, **4**, 13852–13858.

60 J.-S. Nam, K. Kim, J. Han, D. Kim, I. Chung, D. H. Wang and I. Jeon, *ACS Appl. Mater. Interfaces*, 2021, **13**, 42935–42943.

61 Y. Cui, L. Yang, X. Wu, J. Deng, X. Zhang and J. Zhang, *J. Mater. Chem. C*, 2022, **10**, 16629–16656.

62 B.-W. Park, B. Philippe, X. Zhang, H. Rensmo, G. Boschloo and E. Johansson, *Adv. Mater.*, 2015, **27**, 6806–6813.

63 Y. Kim, Z. Yang, A. Jain, O. Voznyy, G. H. Kim, M. Liu, L. N. Quan, F. P. García de Arquer, R. Comin and J. Z. Fan, *Angew. Chem., Int. Ed.*, 2016, **55**, 9586–9590.

64 K. W. Jung, M. R. Sohn, H. M. Lee, I. S. Yang, S. Do Sung, J. Kim, E. W.-G. Diau and W. I. Lee, *Sustainable Energy Fuels*, 2018, **2**, 294–302.

65 M. Khazaee, K. Sardashti, J.-P. Sun, H. Zhou, C. Clegg, I. G. Hill, J. L. Jones, D. C. Lupascu and D. B. Mitzi, *Chem. Mater.*, 2018, **30**, 3538–3544.

66 S. M. Jain, D. Phuyal, M. L. Davies, M. Li, B. Philippe, C. De Castro, Z. Qiu, J. Kim, T. Watson and W. C. Tsoi, *Nano Energy*, 2018, **49**, 614–624.

67 N. Pai, J. Lu, T. R. Gengenbach, A. Seeber, A. S. Chesman, L. Jiang, D. C. Senevirathna, P. C. Andrews, U. Bach and Y. B. Cheng, *Adv. Energy Mater.*, 2019, **9**, 1803396.

68 N. A. Raval and V. Kheraj, *Sol. Energy*, 2025, **286**, 113128.

69 B. Saparov, F. Hong, J.-P. Sun, H.-S. Duan, W. Meng, S. Cameron, I. G. Hill, Y. Yan and D. B. Mitzi, *Chem. Mater.*, 2015, **27**, 5622–5632.

70 J.-C. Hebig, I. Kuhn, J. Flohre and T. Kirchartz, *ACS Energy Lett.*, 2016, **1**, 309–314.

71 K. M. Boopathi, P. Karuppuswamy, A. Singh, C. Hanmandlu, L. Lin, S. A. Abbas, C. C. Chang, P. C. Wang, G. Li and C. W. Chu, *J. Mater. Chem. A*, 2017, **5**, 20843–20850.

72 S. Chatterjee and A. J. Pal, *ACS Appl. Mater. Interfaces*, 2018, **10**, 35194–35205.

73 H. Karmaker, A. Siddique, B. K. Das and M. N. Islam, *Results Eng.*, 2024, **22**, 102106.

74 F. Ji, G. Boschloo, F. Wang and F. Gao, *Sol. RRL*, 2023, **7**, 2201112.

75 J. Kangsabanik, V. Sugathan, A. Yadav, A. Yella and A. Alam, *Phys. Rev. Mater.*, 2018, **2**, 055401.

76 D. B. Mitzi, C. Feild, W. Harrison and A. Guloy, *Nature*, 1994, **369**, 467–469.

77 Y. Su, J. Yang, H. Rao, Y. Zhong, W. Sheng, L. Tan and Y. Chen, *Energy Environ. Sci.*, 2023, **16**, 2177–2186.

78 T. C. Jellicoe, J. M. Richter, H. F. Glass, M. Tabachnyk, R. Brady, S. E. Dutton, A. Rao, R. H. Friend, D. Credgington and N. C. Greenham, *J. Am. Chem. Soc.*, 2016, **138**, 2941–2944.

79 A. Wang, X. Yan, M. Zhang, S. Sun, M. Yang, W. Shen, X. Pan, P. Wang and Z. Deng, *Chem. Mater.*, 2016, **28**, 8132–8140.

80 B. Yang, X. Mao, F. Hong, W. Meng, Y. Tang, X. Xia, S. Yang, W. Deng and K. Han, *J. Am. Chem. Soc.*, 2018, **140**, 17001–17006.

81 M. Xiao, F. Huang, W. Huang, Y. Dkhissi, Y. Zhu, J. Etheridge, A. Gray-Weale, U. Bach, Y. B. Cheng and L. Spiccia, *Angew. Chem., Int. Ed.*, 2014, **53**, 9898–9903.

82 C.-H. Chiang and C.-G. Wu, *Nat. Photonics*, 2016, **10**, 196–200.

83 E. Jokar, P.-Y. Cheng, C.-Y. Lin, S. Narra, S. Shahbazi and E. Wei-Guang Diau, *ACS Energy Lett.*, 2021, **6**, 485–492.

84 F. Hao, C. C. Stoumpos, P. Guo, N. Zhou, T. J. Marks, R. P. Chang and M. G. Kanatzidis, *J. Am. Chem. Soc.*, 2015, **137**, 11445–11452.

85 J. Liu, M. Ozaki, S. Yakumaru, T. Handa, R. Nishikubo, Y. Kanemitsu, A. Saeki, Y. Murata, R. Murdey and A. Wakamiya, *Angew. Chem.*, 2018, **130**, 13405–13409.

86 Z. Zhu, C. C. Chueh, N. Li, C. Mao and A. K. Y. Jen, *Adv. Mater.*, 2018, **30**, 1703800.

87 M. Chen, L. Wan, M. Kong, H. Hu, Y. Gan, J. Wang, F. Chen, Z. Guo, D. Eder and S. Wang, *J. Alloys Compd.*, 2018, **738**, 422–431.

88 X. Liu, T. Wu, X. Luo, H. Wang, M. Furue, T. Bessho, Y. Zhang, J. Nakazaki, H. Segawa and L. Han, *ACS Energy Lett.*, 2021, **7**, 425–431.

89 T. Yokoyama, D. H. Cao, C. C. Stoumpos, T.-B. Song, Y. Sato, S. Aramaki and M. G. Kanatzidis, *J. Phys. Chem. Lett.*, 2016, **7**, 776–782.

90 M. Wang, P. Zeng, S. Bai, J. Gu, F. Li, Z. Yang and M. Liu, *Sol. RRL*, 2018, **2**, 1800217.

91 J. Chen, L. Zuo, Y. Zhang, X. Lian, W. Fu, J. Yan, J. Li, G. Wu, C. Z. Li and H. Chen, *Adv. Energy Mater.*, 2018, **8**, 1800438.

92 G. Schileo and G. Grancini, *J. Mater. Chem. C*, 2021, **9**, 67–76.

93 F. Hao, C. C. Stoumpos, D. H. Cao, R. P. Chang and M. G. Kanatzidis, *Nat. Photonics*, 2014, **8**, 489–494.

94 W. Ke, C. C. Stoumpos, M. Zhu, L. Mao, I. Spanopoulos, J. Liu, O. Y. Kontsevoi, M. Chen, D. Sarma and Y. Zhang, *Sci. Adv.*, 2017, **3**, e1701293.

95 C. C. Stoumpos, C. D. Malliakas and M. G. Kanatzidis, *Inorg. Chem.*, 2013, **52**, 9019–9038.

96 W. Ke, C. C. Stoumpos, I. Spanopoulos, L. Mao, M. Chen, M. R. Wasielewski and M. G. Kanatzidis, *J. Am. Chem. Soc.*, 2017, **139**, 14800–14806.

97 C. Wang, Y. Zhang, F. Gu, Z. Zhao, H. Li, H. Jiang, Z. Bian and Z. Liu, *Matter*, 2021, **4**, 709–721.

98 Y. Liao, H. Liu, W. Zhou, D. Yang, Y. Shang, Z. Shi, B. Li, X. Jiang, L. Zhang and L. N. Quan, *J. Am. Chem. Soc.*, 2017, **139**, 6693–6699.

99 M.-G. Ju, J. Dai, L. Ma, Y. Zhou, W. Liang and X. C. Zeng, *J. Mater. Chem. A*, 2019, **7**, 16742–16747.

100 J. Shin, M. Kim, S. Jung, C. S. Kim, J. Park, A. Song, K.-B. Chung, S.-H. Jin, J. H. Lee and M. Song, *Nano Res.*, 2018, **11**, 6283–6293.

101 Y. Yang, C. Liu, M. Cai, Y. Liao, Y. Ding, S. Ma, X. Liu, M. Guli, S. Dai and M. K. Nazeeruddin, *ACS Appl. Mater. Interfaces*, 2020, **12**, 17062–17069.

102 A. H. Slavney, T. Hu, A. M. Lindenberg and H. I. Karunadasa, *J. Am. Chem. Soc.*, 2016, **138**, 2138–2141.

103 E. Greul, M. L. Petrus, A. Binek, P. Docampo and T. Bein, *J. Mater. Chem. A*, 2017, **5**, 19972–19981.

104 W. Gao, C. Ran, J. Xi, B. Jiao, W. Zhang, M. Wu, X. Hou and Z. Wu, *ChemPhysChem*, 2018, **19**, 1696–1700.

105 C. J. Bartel, C. Sutton, B. R. Goldsmith, R. Ouyang, C. B. Musgrave, L. M. Ghiringhelli and M. Scheffler, *Sci. Adv.*, 2019, **5**, eaav0693.

106 P. C. Harikesh, H. K. Mulmudi, B. Ghosh, T. W. Goh, Y. T. Teng, K. Thirumal, M. Lockrey, K. Weber, T. M. Koh and S. Li, *Chem. Mater.*, 2016, **28**, 7496–7504.

107 J. W. Lee, D. H. Kim, H. S. Kim, S. W. Seo, S. M. Cho and N. G. Park, *Adv. Energy Mater.*, 2015, **5**, 1501310.

108 N. Pellet, P. Gao, G. Gregori, T. Y. Yang, M. K. Nazeeruddin, J. Maier and M. Grätzel, *Angew. Chem., Int. Ed.*, 2014, **53**, 3151–3157.

109 Y. Peng, F. Li, Y. Wang, Y. Li, R. L. Hoye, L. Feng, K. Xia and V. Pecunia, *Appl. Mater. Today*, 2020, **19**, 100637.

110 L. Liang and P. Gao, *Adv. Sci.*, 2018, **5**, 1700331.

111 F. Yang, R. W. MacQueen, D. Menzel, A. Musiienko, A. Al-Ashouri, J. Thiesbrummel, S. Shah, K. Prashanthan, D. Abou-Ras and L. Korte, *Adv. Energy Mater.*, 2023, **13**, 2204339.

112 M. S. Ozório, M. Srikanth, R. Besse and J. L. Da Silva, *Phys. Chem. Chem. Phys.*, 2021, **23**, 2286–2297.

113 T. Ozturk, E. Akman, A. E. Shalan and S. Akin, *Nano Energy*, 2021, **87**, 106157.

114 Z. Fang, M. Shang, X. Hou, Y. Zheng, Z. Du, Z. Yang, K.-C. Chou, W. Yang, Z. L. Wang and Y. Yang, *Nano Energy*, 2019, **61**, 389–396.

115 A. Singh, N.-C. Chiu, K. M. Boopathi, Y.-J. Lu, A. Mohapatra, G. Li, Y.-F. Chen, T.-F. Guo and C.-W. Chu, *ACS Appl. Mater. Interfaces*, 2019, **11**, 35088–35094.

116 T. J. Macdonald, L. Lanzetta, X. Liang, D. Ding and S. A. Haque, *Adv. Mater.*, 2023, **35**, 2206684.

117 N. Ghimire, R. S. Bobba, A. Gurung, K. M. Reza, M. A. R. Laskar, B. S. Lamsal, K. Emshadi, R. Pathak, M. A. Afroz and A. H. Chowdhury, *ACS Appl. Energy Mater.*, 2021, **4**, 1731–1742.

118 J. Zhou, F. Zhao, J. Shen, Y. Zhou, Y. Wu, Y. Guo, J. Jiang and J. Chu, *J. Mater. Chem. C*, 2021, **9**, 15301–15308.

119 Z. Jin, Z. Zhang, J. Xiu, H. Song, T. Gatti and Z. He, *J. Mater. Chem. A*, 2020, **8**, 16166–16188.

120 R. Chiara, M. Morana and L. Malavasi, *ChemPlusChem*, 2021, **86**, 879–888.

121 K. Ahmad, P. Kumar and S. M. Mobin, *Chem. – Asian J.*, 2020, **15**, 2859–2863.

122 K. Ahmad and S. M. Mobin, *ACS Omega*, 2020, **5**, 28404–28412.

123 H. Yao, F. Zhou, Z. Li, Z. Ci, L. Ding and Z. Jin, *Adv. Sci.*, 2020, **7**, 1903540.

124 A. K. Deb and V. Kumar, *AIP Adv.*, 2015, **5**, 077158.

125 M. Konstantakou and T. Stergiopoulos, *J. Mater. Chem. A*, 2017, **5**, 11518–11549.

126 M. Roknuzzaman, K. Ostrikov, H. Wang, A. Du and T. Tesfamichael, *Sci. Rep.*, 2017, **7**, 14025.

127 M. V. Kovalenko, L. Protesescu and M. I. Bodnarchuk, *Science*, 2017, **358**, 745–750.

128 L.-J. Chen, C.-R. Lee, Y.-J. Chuang, Z.-H. Wu and C. Chen, *J. Phys. Chem. Lett.*, 2016, **7**, 5028–5035.

129 G. Wang, J. Chang, J. Bi, M. Lei, C. Wang and Q. Qiao, *Sol. RRL*, 2022, **6**, 2100841.

130 R. Ganesan, S. Vinodhini, V. Balasubramani, G. Parthipan, T. Sridhar, R. Arulmozhi and R. Muralidharan, *New J. Chem.*, 2019, **43**, 15258–15266.

131 M. K. Hossain, M. S. Uddin, G. I. Toki, M. K. Mohammed, R. Pandey, J. Madan, M. F. Rahman, M. R. Islam, S. Bhattarai and H. Bencherif, *RSC Adv.*, 2023, **13**, 23514–23537.

132 B. P. Nguyen, H. R. Jung, K. Y. Ryu, K. Kim and W. Jo, *J. Phys. Chem. C*, 2019, **123**, 30833–30841.

133 B. P. Nguyen, D. Shin, H. R. Jung, J. Kim, T. T. T. Nguyen, S. Yoon, Y. Yi and W. Jo, *Sol. Energy*, 2019, **186**, 136–144.

134 Y. Zhou, D. Yan, H. Zhang, Y. Jing, L. Chao, M. Li, M. Li, Y. Chen, R. Chen and L. Xu, *ACS Mater. Lett.*, 2023, **5**, 2096–2103.

135 Y. Sasaki, M. Murayama and X. Zhao, *ACS Omega*, 2024, **9**, 34339–34344.

136 C. Ferrara, M. Patrini, A. Pisanu, P. Quadrelli, C. Milanese, C. Tealdi and L. Malavasi, *J. Mater. Chem. A*, 2017, **5**, 9391–9395.

137 Z. Zhao, F. Gu, Y. Li, W. Sun, S. Ye, H. Rao, Z. Liu, Z. Bian and C. Huang, *Adv. Sci.*, 2017, **4**, 1700204.

138 T. M. Koh, T. Krishnamoorthy, N. Yantara, C. Shi, W. L. Leong, P. P. Boix, A. C. Grimsdale, S. G. Mhaisalkar and N. Mathews, *J. Mater. Chem. A*, 2015, **3**, 14996–15000.

139 J. Cao, Q. Tai, P. You, G. Tang, T. Wang, N. Wang and F. Yan, *J. Mater. Chem. A*, 2019, **7**, 26580–26585.

140 M. Chen, Q. Dong, F. T. Eickemeyer, Y. Liu, Z. Dai, A. D. Carl, B. Bahrami, A. H. Chowdhury, R. L. Grimm and Y. Shi, *ACS Energy Lett.*, 2020, **5**, 2223–2230.

141 Z. Lin, C. Liu, G. Liu, J. Yang, X. Duan, L. Tan and Y. Chen, *Chem. Commun.*, 2020, **56**, 4007–4010.

142 X. Meng, T. Wu, X. Liu, X. He, T. Noda, Y. Wang, H. Segawa and L. Han, *J. Phys. Chem. Lett.*, 2020, **11**, 2965–2971.

143 W. Żuraw, D. Kubicki, R. Kudrawiec and Ł. Przypis, *ACS Energy Lett.*, 2024, **9**, 4509–4515.

144 J. Ling, D. T. Cuzzupè, M. F. U. Din, A. Stepura, T. Burgard, Y. A. Temitmie, E. Majkova, M. Omastova, R. Jose and L. Schmidt-Mende, *ACS Appl. Energy Mater.*, 2024, **7**, 7152–7158.

145 C.-H. Kuan, T.-S. Liao, S. Narra, Y.-W. Tsai, J.-M. Lin, G.-R. Chen and E. W.-G. Diau, *J. Phys. Chem. Lett.*, 2024, **15**, 7763–7769.

146 W. Zeng, D. Cui, Z. Li, Y. Tang, X. Yu, Y. Li, Y. Deng, R. Ye, Q. Niu and R. Xia, *Sol. Energy*, 2019, **194**, 272–278.

147 L. Peng and W. Xie, *RSC Adv.*, 2020, **10**, 14679–14688.

148 D. Mora-Herrera and M. Pal, *J. Phys. Chem. C*, 2022, **126**, 5847–5862.

149 Z. Zhu, X. Jiang, D. Yu, N. Yu, Z. Ning and Q. Mi, *ACS Energy Lett.*, 2022, **7**, 2079–2083.

150 C. Liu, J. Tu, X. Hu, Z. Huang, X. Meng, J. Yang, X. Duan, L. Tan, Z. Li and Y. Chen, *Adv. Funct. Mater.*, 2019, **29**, 1808059.

151 C. H. Ng, K. Hamada, G. Kapil, M. A. Kamarudin, Z. Wang, Q. Shen, K. Yoshino, T. Minemoto and S. Hayase, *J. Mater. Chem. A*, 2020, **8**, 2962–2968.

152 D. B. Khadka, Y. Shirai, M. Yanagida and K. Miyano, *J. Mater. Chem. C*, 2020, **8**, 2307–2313.

153 J. Li, P. Hu, Y. Chen, Y. Li and M. Wei, *ACS Sustainable Chem. Eng.*, 2020, **8**, 8624–8628.

154 X. Meng, Y. Li, Y. Qu, H. Chen, N. Jiang, M. Li, D. J. Xue, J. S. Hu, H. Huang and S. Yang, *Angew. Chem.*, 2021, **133**, 3737–3742.

155 X. Jiang, F. Wang, Q. Wei, H. Li, Y. Shang, W. Zhou, C. Wang, P. Cheng, Q. Chen and L. Chen, *Nat. Commun.*, 2020, **11**, 1245.

156 M. Li, W.-W. Zuo, Y.-G. Yang, M. Aldamasy, Q. Wang, S. H. T. Cruz, S.-L. Feng, M. Saliba, Z.-K. Wang and A. Abate, *ACS Energy Lett.*, 2020, **5**, 1923–1929.

157 X. Xu, K. Cao, W. Zhu, W. Gu, B. Ma, M. Qin, J. Qian, J. Lu, Z. Liu and S. Chen, *ACS Appl. Energy Mater.*, 2020, **3**, 5415–5426.

158 K. Sekar, L. Marasamy, S. Mayarambakam, P. Selvarajan and J. Bouclé, *Mater. Today Commun.*, 2024, **38**, 108347.

159 P. Kumar, K. Ahmad and S. M. Mobin, *Nano. Adv.*, 2023, **5**, 1624–1630.

160 K. Ahmad, P. Kumar, P. Shrivastava and S. M. Mobin, *Energy Technol.*, 2022, **10**, 2100717.

161 S. Vijaya, J. Subbiah, D. J. Jones and S. Anandan, *RSC Adv.*, 2023, **13**, 9978–9982.

162 F. Li, Y. Wang, K. Xia, R. L. Hoye and V. Pecunia, *J. Mater. Chem. A*, 2020, **8**, 4396–4406.

163 X. Meng, Y. Wang, J. Lin, X. Liu, X. He, J. Barbaud, T. Wu, T. Noda, X. Yang and L. Han, *Joule*, 2020, **4**, 902–912.

164 S. M. Jain, T. Edvinsson and J. R. Durrant, *Commun. Chem.*, 2019, **2**, 91.

165 M. A. Karim, M. Matsuishi, T. H. Chowdhury, W. I. Chowdhury, M. Abdel-shakour and A. Islam, *J. Mater. Sci.: Mater. Electron.*, 2022, **33**, 8114–8126.

166 K. Ahmad, S. N. Ansari, K. Natarajan and S. M. Mobin, *ChemElectroChem*, 2019, **6**, 1192–1198.

167 S. Sanders, D. Stümmler, P. Pfeiffer, N. Ackermann, G. Simkus, M. Heuken, P. Baumann, A. Vescan and H. Kalisch, *Sci. Rep.*, 2019, **9**, 9774.

168 M.-C. Tang, D. Barrit, R. Munir, R. Li, J. M. Barbé, D.-M. Smilgies, S. Del Gobbo, T. D. Anthopoulos and A. Amassian, *Sol. RRL*, 2019, **3**, 1800305.

169 C. Lan, G. Liang, S. Zhao, H. Lan, H. Peng, D. Zhang, H. Sun, J. Luo and P. Fan, *Sol. Energy*, 2019, **177**, 501–507.

170 S. Weber, T. Rath, K. Fellner, R. Fischer, R. Resel, B. Kunert, T. Dimopoulos, A. Steinegger and G. Trimmel, *ACS Appl. Energy Mater.*, 2018, **2**, 539–547.

171 K. Ahmad, P. Kumar and S. M. Mobin, *ChemElectroChem*, 2020, **7**, 946–950.

172 P. Kumar, K. Ahmad, J. Dagar, E. Unger and S. M. Mobin, *ChemElectroChem*, 2021, **8**, 3150–3154.

173 M. Chen, Q. Dong, C. Xiao, X. Zheng, Z. Dai, Y. Shi, J. M. Luther and N. P. Padture, *ACS Energy Lett.*, 2022, **7**, 2256–2264.

174 M. Chen, M.-G. Ju, H. F. Garces, A. D. Carl, L. K. Ono, Z. Hawash, Y. Zhang, T. Shen, Y. Qi and R. L. Grimm, *Nat. Commun.*, 2019, **10**, 16.

175 Y. Raoui, S. Kazim, Y. Galagan, H. Ez-Zahraouy and S. Ahmad, *Sustainable Energy Fuels*, 2021, **5**, 4661–4667.

176 M. Kong, O. Raievska, O. Stroyuk, A. Barabash, Z. Wu, J. Tian, C. Erban, A. Osvet, M. Batentschuk and C. J. Brabec, *ACS Appl. Mater. Interfaces*, 2024, **16**, 43713–43723.

177 P. Huang, M. Sheokand, D. Payno Zarceño, S. Kazim, L. Lezama, M. K. Nazeeruddin, R. Misra and S. Ahmad, *ACS Appl. Energy Mater.*, 2023, **6**, 7955–7964.

178 K. Sekar, L. Marasamy, S. Mayarambakam, H. Hawashin, M. Nour and J. Bouclé, *RSC Adv.*, 2023, **13**, 25483–25496.

179 Z. Zhang, Q. Sun, Y. Lu, F. Lu, X. Mu, S.-H. Wei and M. Sui, *Nat. Commun.*, 2022, **13**, 3397.

180 F. Igbari, R. Wang, Z.-K. Wang, X.-J. Ma, Q. Wang, K.-L. Wang, Y. Zhang, L.-S. Liao and Y. Yang, *Nano Lett.*, 2019, **19**, 2066–2073.

181 M. Ghasemi, L. Zhang, J. H. Yun, M. Hao, D. He, P. Chen, Y. Bai, T. Lin, M. Xiao and A. Du, *Adv. Funct. Mater.*, 2020, **30**, 2002342.

182 M. K. Hossain, D. Samajdar, R. C. Das, A. Arnab, M. F. Rahman, M. Rubel, M. R. Islam, H. Bencherif, R. Pandey and J. Madan, *Energy Fuels*, 2023, **37**, 3957–3979.

183 C. Gao, X. Wang, Q. Yang, C. Gao, X. Wang and X. Liu, *J. Phys. Chem. Lett.*, 2024, **15**, 8896–8902.

184 C. C. Stoumpos, L. Frazer, D. J. Clark, Y. S. Kim, S. H. Rhim, A. J. Freeman, J. B. Ketterson, J. I. Jang and M. G. Kanatzidis, *J. Am. Chem. Soc.*, 2015, **137**, 6804–6819.

185 R. Chen, C. Liu, Y. Chen, C. Ye, S. Chen, J. Cheng, S. Cao, S. Wang, A. Cui and Z. Hu, *J. Phys. Chem. C*, 2022, **127**, 635–641.

186 J. Qian, B. Xu and W. Tian, *Org. Electro*, 2016, **37**, 61–73.

187 C. H. Ng, K. Nishimura, N. Ito, K. Hamada, D. Hirotani, Z. Wang, F. Yang, Q. Shen, K. Yoshino and T. Minemoto, *Nano Energy*, 2019, **58**, 130–137.

188 K. Ahmad, S. N. Ansari, K. Natarajan and S. M. Mobin, *ACS Appl. Energy Mater.*, 2018, **1**, 2405–2409.

189 N. Pradhan, S. Das Adhikari, A. Nag and D. Sarma, *Angew. Chem., Int. Ed.*, 2017, **56**, 7038–7054.

190 A. K. Jena, A. Kulkarni and T. Miyasaka, *Chem. Rev.*, 2019, **119**, 3036–3103.

191 H. Lei, D. Hardy and F. Gao, *Adv. Funct. Mater.*, 2021, **31**, 2105898.

192 P. Zhang, J. Yang and S.-H. Wei, *J. Mater. Chem. A*, 2018, **6**, 1809–1815.

193 S. Zhao, K. Yamamoto, S. Iikubo, S. Hayase and T. Ma, *J. Phys. Chem. Solids*, 2018, **117**, 117–121.

194 G. Volonakis, M. R. Filip, A. A. Haghighirad, N. Sakai, B. Wenger, H. J. Snaith and F. Giustino, *J. Phys. Chem. Lett.*, 2016, **7**, 1254–1259.

195 T. J. Jacobsson, M. Pazoki, A. Hagfeldt and T. Edvinsson, *J. Phys. Chem. C*, 2015, **119**, 25673–25683.

196 X.-P. Cui, K.-J. Jiang, J.-H. Huang, Q.-Q. Zhang, M.-J. Su, L.-M. Yang, Y.-L. Song and X.-Q. Zhou, *Synth. Met.*, 2015, **209**, 247–250.

197 D. Cortecchia, H. A. Dewi, J. Yin, A. Bruno, S. Chen, T. Baikie, P. P. Boix, M. Grätzel, S. Mhaisalkar and C. Soci, *Inorg. Chem.*, 2016, **55**, 1044–1052.

198 K. Ahmad and S. M. Mobin, *Energy Technol.*, 2020, **8**, 1901185.

199 M. F. Mostafa and R. D. Willett, *Phys. Rev. B*, 1971, **4**, 2213.

200 X. Zhang, J. Yin, Z. Nie, Q. Zhang, N. Sui, B. Chen, Y. Zhang, K. Qu, J. Zhao and H. Zhou, *RSC Adv.*, 2017, **7**, 37419–37425.

201 M.-G. Ju, M. Chen, Y. Zhou, H. F. Garces, J. Dai, L. Ma, N. P. Padture and X. C. Zeng, *ACS Energy Lett.*, 2018, **3**, 297–304.

202 Z. Xiao, Z. Song and Y. Yan, *Adv. Mater.*, 2019, **31**, 1803792.

203 B. Ghosh, B. Wu, H. K. Mulmudi, C. Guet, K. Weber, T. C. Sum, S. Mhaisalkar and N. Mathews, *ACS Appl. Mater. Interfaces*, 2018, **10**, 35000–35007.

204 F. Jiang, D. Yang, Y. Jiang, T. Liu, X. Zhao, Y. Ming, B. Luo, F. Qin, J. Fan and H. Han, *J. Am. Chem. Soc.*, 2018, **140**, 1019–1027.

205 H. Cho, S.-H. Jeong, M.-H. Park, Y.-H. Kim, C. Wolf, C.-L. Lee, J. H. Heo, A. Sadhanala, N. Myoung and S. Yoo, *Science*, 2015, **350**, 1222–1225.

206 H. Wang, C. Zhang, W. Huang, X. Zou, Z. Chen, S. Sun, L. Zhang, J. Li, J. Cheng and S. Huang, *Phys. Chem. Chem. Phys.*, 2022, **24**, 27585–27605.

207 A. W. Ho-Baillie, J. Zheng, M. A. Mahmud, F.-J. Ma, D. R. McKenzie and M. A. Green, *Appl. Phys. Rev.*, 2021, **8**, 041307.

208 K. O. Brinkmann, P. Wang, F. Lang, W. Li, X. Guo, F. Zimmermann, S. Olthof, D. Neher, Y. Hou and M. Stolterfoht, *Nat. Rev. Mater.*, 2024, **9**, 202–217.

209 N. Shrivastav, J. Madan and R. Pandey, *Ind. J. Phys*, 2024, 1–9.

210 Q. Han, Y.-T. Hsieh, L. Meng, J.-L. Wu, P. Sun, E.-P. Yao, S.-Y. Chang, S.-H. Bae, T. Kato and V. Bermudez, *Science*, 2018, **361**, 904–908.

211 K. Amri, R. Belghouthi, M. Aillerie and R. Gharbi, *Energies*, 2021, **14**, 3383.

212 A. Al-Ashouri, E. Köhnen, B. Li, A. Magomedov, H. Hempel, P. Caprioglio, J. A. Márquez, A. B. Morales Vilches, E. Kasparavicius and J. A. Smith, *Science*, 2020, **370**, 1300–1309.

213 T. Serikova, G. Bizhanova, H. Hu and A. Ng, *Bullet. Karaganda Univ. Phys. Series*, 2023, **111**, 6–15.

214 X. Chen, Z. Jia, Z. Chen, T. Jiang, L. Bai, F. Tao, J. Chen, X. Chen, T. Liu and X. Xu, *Joule*, 2020, **4**, 1594–1606.

215 T. Duong, Y. Wu, H. Shen, J. Peng, X. Fu, D. Jacobs, E. C. Wang, T. C. Kho, K. C. Fong and M. Stocks, *Adv. Energy Mater.*, 2017, **7**, 1700228.

216 K. A. Bush, A. F. Palmstrom, Z. J. Yu, M. Boccard, R. Cheacharoen, J. P. Mailoa, D. P. McMeekin, R. L. Hoye, C. D. Bailie and T. Leijtens, *Nat. Energy*, 2017, **2**, 1–7.

217 Z. Zhu, K. Mao and J. Xu, *J. Chem.*, 2021, **58**, 219–232.

218 T. Leijtens, R. Prasanna, K. A. Bush, G. E. Eperon, J. A. Raiford, A. Gold-Parker, E. J. Wolf, S. A. Swifter, C. C. Boyd and H.-P. Wang, *Sustainable Energy Fuels*, 2018, **2**, 2450–2459.

219 I. Kopacic, B. Friesenbichler, S. F. Hoefler, B. Kunert, H. Plank, T. Rath and G. Trimmel, *ACS Appl. Energy Mater.*, 2018, **1**, 343–347.

220 X. Wang, T. Zhang, Y. Lou and Y. Zhao, *Mater. Chem. Front.*, 2019, **3**, 365–375.

221 S. Gupta, T. Bendikov, G. Hodes and D. Cahen, *ACS Energy Lett.*, 2016, **1**, 1028–1033.

222 C. Gong, H. Li, Z. Xu, Y. Li, H. Wang, Q. Zhuang, A. Wang, Z. Li, Z. Guo and C. Zhang, *Nat. Commun.*, 2024, **15**, 9154.

223 S. Joy, H. R. Atapattu, S. Sorensen, H. Pruett, A. B. Olivelli, A. J. Huckaba, A.-F. Miller and K. R. Graham, *J. Mater. Chem. A*, 2022, **10**, 13278–13285.

224 D. Nematov, I. Raufov, A. Ashurov, S. Sattorzoda, T. Najmiddinov, S. Nazriddinzoda, M. Umarzoda and K. Yusupova, *International Journal of Research and Innovation in Applied Science*, 2025, 353–377.

225 S. Sajid, S. Alzahmi, I. B. Salem, N. Tabet, Y. Haik and I. M. Obaidat, *Mater. Renewable Sustainable Energy*, 2024, **13**, 133–153.

226 Y.-L. Liu, C.-L. Yang, M.-S. Wang, X.-G. Ma and Y.-G. Yi, *J. Mater. Sci.*, 2019, **54**, 4732–4741.

227 A. Singh, K. M. Boopathi, A. Mohapatra, Y. F. Chen, G. Li and C. W. Chu, *ACS Appl. Mater. Interfaces*, 2018, **10**, 2566–2573.

228 Z. Zhang, X. Li, X. Xia, Z. Wang, Z. Huang, B. Lei and Y. Gao, *J. Phys. Chem. Lett.*, 2017, **8**, 4300–4307.

229 P. Karuppuswamy, K. M. Boopathi, A. Mohapatra, H.-C. Chen, K.-T. Wong, P.-C. Wang and C.-W. Chu, *Nano Energy*, 2018, **45**, 330–336.

230 C. Ran, Z. Wu, J. Xi, F. Yuan, H. Dong, T. Lei, X. He and X. Hou, *J. Phys. Chem. Lett.*, 2017, **8**, 394–400.

231 Z. Liu, M. Chen, L. Wan, Y. Liu, Y. Wang, Y. Gan, Z. Guo, D. Eder and S. Wang, *SN Appl. Sci.*, 2019, **1**, 1–11.

232 M. H. Miah, M. U. Khandaker, M. B. Rahman, M. Nur-E-Alam and M. A. Islam, *RSC Adv.*, 2024, **14**, 15876–15906.

233 P. Baraneedharan, S. Sekar, S. Murugesan, D. Ahamada, S. A. B. Mohamed, Y. Lee and S. Lee, *Nanomaterials*, 2024, **14**, 1867.

234 T. Cai, W. Shi, R. Wu, C. Chu, N. Jin, J. Wang, W. Zheng, X. Wang and O. Chen, *J. Am. Chem. Soc.*, 2024, **146**, 3200–3209.

235 W. Żuraw, F. A. Vinocour Pacheco, J. Sánchez-Diaz, Ł. Przypis, M. A. Mejia Escobar, S. Almosni, G. Vescio, J. P. Martínez-Pastor, B. Garrido and R. Kudrawiec, *ACS Energy Lett.*, 2023, **8**, 4885–4887.

236 E. Aktas, N. Rajamanickam, J. Pascual, S. Hu, M. H. Aldamasy, D. Di Girolamo, W. Li, G. Nasti, E. Martínez-Ferrero and A. Wakamiya, *Commun. Mater.*, 2022, **3**, 104.

237 T. Dai, Q. Cao, L. Yang, M. H. Aldamasy, M. Li, Q. Liang, H. Lu, Y. Dong and Y. Yang, *Crystals*, 2021, **11**, 295.

238 A. D. Khan, M. Mustajab, S. Moeen, M. Imran, M. Ikram, Q. Khan and M. Khan, *Environ. Sci. Adv.*, 2024, **3**, 1004–1029.